Annu. Rev. Astron. Astrophys. 2003. 41:241–89
doi: 10.1146/annurev.astro.41.011802.094840

First published online as a Review in Advance on June 4, 2003

INTERSTELLAR DUST GRAINS

B.T. Draine
Princeton University Observatory, Princeton, New Jersey 08544;
email: draine@astro.princeton.edu

Key Words infrared astronomy, interstellar medium, interstellar grains, light scattering, molecular clouds

■ **Abstract** This review surveys the observed properties of interstellar dust grains: the wavelength-dependent extinction of starlight, including absorption features, from UV to infrared; optical luminescence; infrared emission; microwave emission; optical, UV, and X-ray scattering by dust; and polarization of starlight and of infrared emission. The relationship between presolar grains in meteorites and the interstellar grain population is discussed. Candidate grain materials and abundance constraints are considered. A dust model consisting of amorphous silicate grains, graphite grains, and polycyclic aromatic hydrocarbons is compared with observed emission and scattering. Some issues concerning evolution of interstellar dust are discussed.

1. INTRODUCTION

Dust grains play a central role in the astrophysics of the interstellar medium, from the thermodynamics and chemistry of the gas to the dynamics of star formation. In addition, dust shapes the spectra of galaxies: Radiation at short wavelengths is attenuated, and energy is radiated in the infrared. It is estimated that 30% or more of the energy emitted as starlight in the Universe is reradiated by dust in the infrared (Bernstein et al. 2002). Interstellar dust determines what galaxies look like, how the interstellar medium (ISM) in a galaxy behaves, and the very process of star formation that creates a visible galaxy.

This review summarizes current knowledge of the abundance, composition, and sizes of interstellar dust grains, as indicated by observations of extinction, scattering, and emission from dust, supplemented by evidence from interstellar gas phase abundances and presolar grains in meteorites. The term "dust grain" is understood here to extend down to molecules containing tens of atoms, as there is no discontinuity in the physics as the particle size decreases from microns to Angstroms.

The distribution of gas and dust in the Galaxy—the structure of the interstellar medium—is not discussed.

The astrophysics of interstellar dust is not covered in this review. This includes the physical optics of small particles, charging of dust grains, heating and cooling of dust grains, chemistry on dust grain surfaces, forces and torques on dust grains,

sputtering and shattering of dust grains, and alignment of dust with the magnetic field; an introduction to these topics can be found elsewhere (Krügel 2002, Draine 2003).

The review does not attempt to survey or compare different models proposed for interstellar dust. One dust model is introduced to illustrate modeling of absorption, scattering, and infrared emission from interstellar dust.

It is not possible to cite all of the important papers in this area; only a few articles are cited in connection with each topic. The reader is encouraged to also consult prior reviews by Savage & Mathis (1979), Mathis (1990, 1993, 2000), Draine (1995), Witt (2000a,b), Voshchinnikov (2002), and the book by Whittet (2003). Dorschner & Henning (1995) discuss the metamorphosis of interstellar dust.

2. EXTINCTION

The existence of interstellar dust was first inferred from obscuration, or "extinction," of starlight (Trumpler 1930). Much of our knowledge of interstellar dust continues to be based on studies of the wavelength-dependence of this attenuation, often referred to as reddening because of the tendency for the extinction to be greater in the blue than in the red. The wavelength-dependence strongly constrains the grain size distribution, and spectral features (see Section 3) reveal the chemical composition.

The extinction is most reliably determined using the pair method—comparing spectrophotometry of two stars of the same spectral class; if one star has negligible foreground dust while the second star is heavily reddened, comparison of the two spectra, together with the assumption that the dust extinction goes to zero at very long wavelength, allows one to determine the extinction $A_\lambda \equiv 2.5 \log_{10}(F_\lambda^0/F_\lambda)$ as a function of wavelength λ, where F_λ is the observed flux and F_λ^0 is the flux in the absence of extinction. The pair method has been used to measure extinction curves for many sightlines, in many cases over a range of wavelengths extending from the near-infrared to the vacuum UV.

2.1. Milky Way Dust

2.1.1. OPTICAL-UV EXTINCTION CURVES The dimensionless quantity $R_V \equiv A_V/(A_B - A_V)$ is a common measure of the slope of the extinction curve in the optical region. Very large grains would produce gray extinction with $R_V \to \infty$. Rayleigh scattering ($A_\lambda \propto \lambda^{-4}$) would produce very steep extinction with $R_V \approx 1.2$. R_V is known to vary from one sightline to another, from values as low as 2.1 (toward HD 210121) (Welty & Fowler 1992) to values as large as 5.6–5.8 (toward HD 36982) (Cardelli et al. 1989, Fitzpatrick 1999). Cardelli et al. (1989) showed that normalized extinction curves A_λ/A_I (using the I band extinction to normalize) could be approximated by a seven-parameter function of wavelength λ:

$$A_\lambda/A_I \approx f(\lambda; R_V, C_1, C_2, C_3, C_4, \lambda_0, \gamma). \quad (1)$$

At wavelengths $\lambda > 3030$ Å, the function $f(\lambda)$ depends only on λ and the single parameter R_V. The parameters C_3, λ_0, and γ determine the strength and shape of the 2175 Å "bump," and the coefficients C_1, C_2, and C_4 determine the slope and curvature of the continuous extinction at $\lambda < 3030$ Å.

Cardelli et al. (1989) show that if the single quantity R_V is known, it is possible to estimate the values of the other six parameters (C_{1-4}, λ_0, γ) so that the optical-UV extinction can be approximated by a one-parameter family of curves. However, if the UV extinction has been measured, an improved fit to the observations can be obtained by fitting C_{1-4}, λ_0 and γ to the measured extinction.

Empirical extinction curves in diffuse clouds show relatively little variation in the infrared, and for wavelengths $0.7\ \mu\text{m} \lesssim \lambda \lesssim 8\ \mu$m the function (1) appears to be approximately "universal" (i.e., independent of R_V) in diffuse clouds [in dense clouds grains acquire "ice" mantles (see Section 3.5) that alter the extinction]. Fitzpatrick (1999) pays careful attention to the effects of finite-width photometric bandpasses and gives modified formulae that appear to improve the overall fit to observations of ice-free dust. The Cardelli et al. (1989) and Fitzpatrick (1999) fits for $R_V = 3.1$ are compared in Section 8 (see Table 4).

Figure 1 shows extinction curves calculated using the Fitzpatrick (1999) parametrization for $R_V = 2.1$, 2.5, 3.1, 4.0, and 5.5. The coefficients in the Cardelli et al. (1989) or Fitzpatrick (1999) fitting formulae can be adjusted to improve the

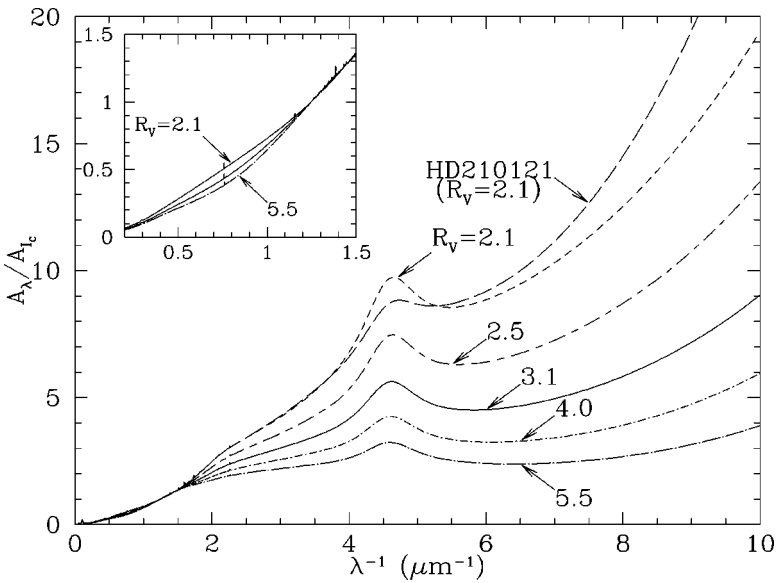

Figure 1 Extinction curves from prescription of Fitzpatrick (1999), with diffuse interstellar bands (DIBs) added as described in Section 3.3. The DIBs are barely visible on this plot.

fit to specific sightlines; such a fit is shown for the extreme case of HD 210121, showing that the UV extinction can differ significantly from the average behavior for the same value of R_V.

"Pair method" determinations of the reddening law for many sightlines indicate that $R_V \approx 3.1$ for the average extinction law for diffuse regions in the local Milky Way (Savage & Mathis 1979, Cardelli et al. 1989). Sightlines intersecting clouds with larger extinction per cloud tend to have larger values of R_V; the larger R_V values may indicate grain growth by accretion and coagulation.

Another approach to determining the wavelength-dependent extinction is to use star counts or galaxy counts as a function of apparent brightness. Szomoru & Guhathakurta (1999) use UBVRI photometry of Galactic field stars to determine the extinction law; for the four high-latitude clouds they studied, they conclude that $R_V \lesssim 2$, well below the value $R_V \approx 3.1$, which is widely considered to be average and comparable to the most extreme values of R_V ever found in studies of individual stars ($R_V = 2.1$ for HD 210121). Further study is needed to reconcile this apparent conflict.

Udalski (2002) uses V and I photometry of "red clump giants" to study the reddening law. Toward the LMC he infers $R_V \approx 3.1$, but toward Galactic bulge regions he finds $R_V \approx 1.8$–2.5.

Sloan Digital Sky Survey (SDSS) photometry (Lupton et al. 2003) can be used to study the reddening toward stars at the "blue tip" of the main sequence (Finkbeiner et al. 2003b). The observed reddening appears to be consistent with $R_V \approx 3.1$. Galaxy surface brightnesses can also be used; SDSS galaxy photometry is consistent with $R_V = 3.1$ (Schlegel et al. 2003).

2.1.2. EXTINCTION PER H Using H Lyman-α and absorption lines of H_2 to determine the total H column density, $N_{\rm H}$, Bohlin et al. (1978) found

$$N_{\rm H}/(A_B - A_V) = 5.8 \times 10^{21}\,{\rm cm}^{-2}\,{\rm mag}^{-1}, \tag{2}$$

$$N_{\rm H}/A_V \approx 1.87 \times 10^{21}\,{\rm cm}^{-2}\,{\rm mag}^{-1} \quad \text{for} \quad R_V = 3.1, \tag{3}$$

to be representative of dust in diffuse regions. For $R_V = 3.1$, the Fitzpatrick (1999) reddening fit gives $A_{I_C}/A_V = 0.554$ for Cousins I band ($\lambda = 0.802\ \mu$m), thus

$$A_{I_C}/N_{\rm H} \approx 2.96 \times 10^{-22}\,{\rm mag\,cm}^2 \quad \text{for} \quad R_V = 3.1. \tag{4}$$

If the extinction curve is really universal for $\lambda \gtrsim 0.7\ \mu$m we might expect Equation 4 to apply independent of R_V. Rachford et al. (2002) report H and H_2 column densities for 16 sightlines through diffuse and translucent clouds. Figure 2 shows $A_{I_C}/N_{\rm H}$ versus R_V^{-1} for the 14 sightlines with $N_{\rm H}$ known to better than a factor 1.5. The I_C band extinction A_{I_C} has been estimated from $A_B - A_V$ and R_V using the Fitzpatrick (1999) R_V-dependent reddening law.

Figure 2 appears to show that $A_{I_C}/N_{\rm H}$ is not universal for local Milky Way dust: the I band extinction per H deviates from Equation 4 when R_V deviates from

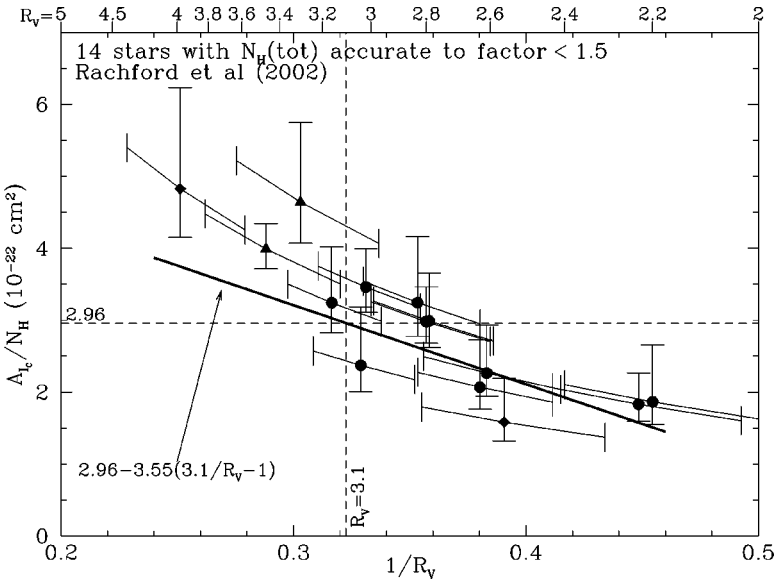

Figure 2 $A_{I_C}/N_{\rm H}$ for 14 sightlines through translucent clouds (Rachford et al. 2002), as a function of $1/R_V$, with R_V determined by IR photometry (circles, $R_V \pm 0.2$); polarization $\lambda_{\rm max}$ (triangles, $R_V \pm 10\%$); or UV extinction curve (diamonds, $R_V \pm 10\%$). Vertical error bars show 1-σ uncertainty due to errors in $N_{\rm H}$; tilted error bars show effects of errors in R_V. Least-squares fit [Equation 5] is shown.

3.1, in the sense that $A_{I_C}/N_{\rm H}$ increases when R_V is larger (larger grains). We note that the trend in $A_{I_C}/N_{\rm H}$ could be in part the result of errors in determination of R_V, (i.e., errors in estimating A_V because $E(B-V)$ is probably accurate to better than 10% for these stars), but the data appear to show a real trend. A least-squares fit, constrained to pass through Equation 4, gives

$$A_{I_C}/N_{\rm H} \approx [2.96\text{–}3.55\,(3.1/R_V - 1)] \times 10^{-22}\,{\rm mag\,cm^2}. \qquad (5)$$

Figure 3 shows $A_\lambda/N_{\rm H}$, the extinction per H, estimated from the Fitzpatrick (1999) extinction fits and Equation 5. If the Fitzpatrick (1999) extinction fits and Equation 5 are both correct, the extinction per H increases for $\lambda \gtrsim 0.3\ \mu$m when R_V increases. Presumably this is due to increased scattering by the grains as the grain size increases.

2.1.3. INFRARED EXTINCTION Between $\sim$0.9 μm and $\sim$5 μm the continuous extinction curve can be approximated by a power-law, $A_\lambda \propto \lambda^{-\beta}$, with $\beta \approx 1.61$ (Rieke & Lebofsky 1985), 1.70 (Whittet 1988), 1.75 (Draine 1989b), $\sim$1.8 (Martin & Whittet 1990), $\sim$1.8 (Whittet et al. 1993), or 1.70 (Bertoldi et al. 1999, Rosenthal et al. 2000).

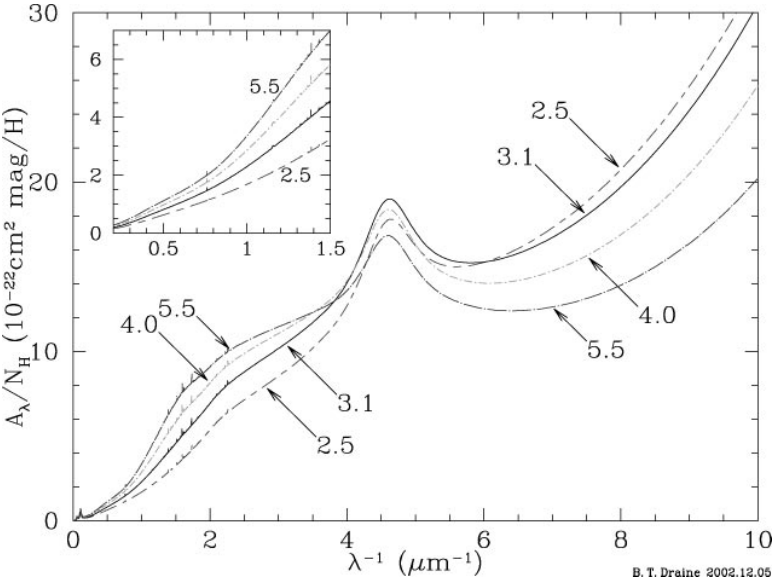

Figure 3 $A_\lambda/N_{\rm H}$ for different values of R_V, using Fitzpatrick (1999) extinction curve fit and $A_I/N_{\rm H}$ from Equation (5).

The extinction in the 5–8 μm region is controversial (see Figure 4). Draine (1989b) concluded that the observational evidence was consistent with $A_\lambda \propto \lambda^{-1.75}$ out to $\lambda \approx 6$ μm. Using ISO observations of H recombination lines, Lutz et al. (1996) find that the extinction toward Sgr A* does not decline with increasing λ in the 4–8 μm region. However, studies using H_2 rovibrational lines in the Orion molecular cloud, (Bertoldi et al. 1999, Rosenthal et al. 2000) find that the extinction continues to decline with increasing λ to a minimum at $\sim$6.5 μm. The wavelength dependence of the continuous dust extinction in the Orion molecular cloud could conceivably differ from that on the sightline to Sgr A*; alternatively, perhaps the H recombination line intensity ratios differ from the "case B" recombination assumed by Lutz et al. It is interesting to see in Figure 4 that the Weingartner & Draine (2001a) grain model for $R_V = 5.5$ is in rough agreement with the Lutz et al. results toward the galactic center. Further observational study of the 5–8 μm extinction is needed. In addition to this continuous extinction, there are strong absorption features at 9.7 μm and 18 μm due to silicates (see Section 3.2), a hydrocarbon feature at 3.4 μm (see Section 3.4), and PAH absorption at 6.2 μm (see Section 3.6). The extinction in molecular clouds also shows additional bands due to ice mantles (see Section 3.5).

2.2. Dust in Other Galaxies

Dust in the Milky Way varies from one sightline to another. It is obviously of great interest to study the dust in other galaxies, both in order to correct

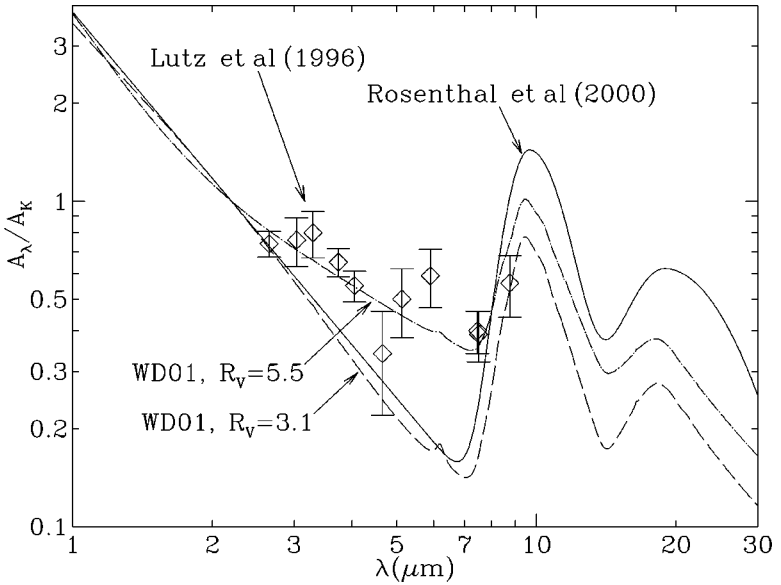

Figure 4 Infrared extinction, relative to extinction at K (2.2 μm), inferred by Rosenthal et al. (2000) for dust in the OMC-1 molecular cloud and by Lutz et al. (1996) for dust toward Sgr A*, and as calculated for the Weingartner & Draine (2001a) grain models for $R_V = 3.1$ (60 ppm C in PAH) and $R_V = 5.5$ (30 ppm C in PAH). The 6.2 μm absorption feature in the WD01 grain models is due to PAHs.

observations for the extinction by the dust and to inform our understanding of dust astrophysics.

Our knowledge of the extinction law for dust in other galaxies is greatest for the Large and Small Magellanic Clouds (LMC and SMC), where we can study the extinction for individual stars, but some progress has been made in determining the wavelength-dependence of extinction in more distant galaxies.

2.2.1. MAGELLANIC CLOUDS Not surprisingly, there are regional variations within the LMC and SMC. Stars more than ∼500 pc away from the 30 Doradus region of the LMC have $R_V \approx 3.2$ and an extinction law that appears to be quite similar to the Milky Way diffuse cloud extinction law (Fitzpatrick 1986, Misselt et al. 1999). The reddening per H atom $E(B-V)/N_{\rm H} \approx 4.5 \times 10^{-23}\,{\rm cm}^2/{\rm H}$ (Koorneef 1982, Fitzpatrick 1985), approximately 26% of the Milky Way value. This is approximately consistent with the LMC metallicity: LMC H II regions have Ne/H $\approx (3.5 \pm 1.4) \times 10^{-5}$ (Kurt & Dufour 1998), ∼30% of the solar Ne/H ($=1.2 \times 10^{-4}$) (Grevesse & Sauval 1998). Stars in or near 30 Dor have extinction curves that have a weakened 2175 Å feature (Fitzpatrick 1986, Misselt et al. 1999).

In the SMC, stars in the "bar" region have extinction curves which appear to lack the 2175 Å feature. The reddening per H is only $E(B-V)/N_{\rm H} = 2.2 \times$

10^{-23} cm^2/H, (Martin et al. 1989) ∼13% of the Milky Way value, again consistent with the SMC metallicity: SMC H II regions have Ne/H $\approx (1.6 \pm 0.2) \times 10^{-5}$ (Dufour 1984, Kurt & Dufour 1998), or 14% of the solar Ne/H, and the gas-phase C/H is only 6% of solar.

Weingartner & Draine (2001a) are able to reproduce the observed extinction laws in the LMC and SMC using appropriate mixtures of carbonaceous and silicate grains. The sightlines in the SMC bar that lack the 2175 Å extinction feature can be reproduced by models that lack carbonaceous grains with radii $a \lesssim 0.02\ \mu$m.

2.2.2. M31 Bianchi et al. (1996) present UV extinction curves toward selected bright stars in M31, finding an extinction law similar to the average Milky Way extinction curve, but with the 2175 Å feature possibly somewhat weaker than in the Milky Way.

2.2.3. OTHER GALAXIES There are several different approaches to determining the extinction curve for dust in galaxies where individual stars cannot be resolved.

The dust extinction law can be determined when a foreground galaxy overlaps a background galaxy. Berlind et al. (1997) find the extinction curve for dust in the spiral arm of NGC 2207 to resemble the Milky Way extinction law for $R_V = 5.0$; the interarm dust appears to be even grayer. However, the flatness of the extinction curve could be due in part to unresolved optically thick dust patches in the foreground galaxy.

Keel & White (2001a) find the extinction law in the spiral galaxy AM 1316-241 to be close to the Milky Way mean extinction, with $R_V = 3.4 \pm 0.2$; for the spiral galaxy AM 0500-620, the dust extinction law appears to be somewhat steeper than the Milky Way average, with $R_V \approx 2.5 \pm 0.4$. Keel & White (2001b) find the extinction law in the Sc galaxy NGC 3314A to be close to the Milky Way mean, with $R_V = 3.5 \pm 0.2$ over galactocentric radii 1.6–3.8 kpc, with no evidence for any radial trend in reddening law.

From observations of the overall emission spectrum Calzetti (2001) infers the internal extinction by dust in starburst galaxies. The inferred reddening law is relatively gray compared to the Galactic reddening law, and shows no evidence of a 2175 Å feature. It is not clear to what extent the flatness of the apparent reddening law may be due to the effects of radiative transfer in optically thick distributions of stars and dust.

Searches have been made for the 2175 Å extinction feature in QSO spectra (McKee & Petrosian 1974). Malhotra (1997) reports a statistical detection in a sample of 92 QSOs, but Pitman et al. (2000) argue that the detection was not statistically significant.

Gravitationally lensed QSOs with multiple images can be used to determine the extinction law if the intrinsic spectrum is assumed to be time independent. Falco et al. (1999) determine extinction laws in galaxies out to $z = 1.01$, with R_V estimates from 1.5 to 7.2. Toft et al. (2000) find the extinction curve in a galaxy at $z = 0.44$ to have $1.3 \lesssim R_V \lesssim 2.0$. Motta et al. (2002) find that the dust in a

lensing galaxy at $z = 0.83$ is consistent with a standard Milky Way extinction law for $R_V = 2.1 \pm 0.9$, including an extinction bump at 2175 Å.

3. SPECTROSCOPY OF DUST

The composition of interstellar dust remains controversial. Although meteorites (see Section 4) provide us with genuine specimens of interstellar grains for examination, these are subject to severe selection effects and cannot be considered representative of interstellar grains. Our only direct information on the composition of interstellar dust comes from spectral features in extinction, scattering, or emission.

3.1. 2175 Å Feature: Aromatic C?

By far the strongest spectral feature is the broad bump in the extinction curve centered at ~2175 Å (see Figure 1).

Fitzpatrick & Massa (1986) showed that the observed 2175 Å feature can be accurately fit with a Drude profile

$$\Delta C_{\rm ext}(\lambda) = \frac{C_0 \gamma^2}{(\lambda/\lambda_0 - \lambda_0/\lambda)^2 + \gamma^2}, \tag{6}$$

peaking at $\lambda_0 = 2175$ Å (or $\lambda_0^{-1} = 4.60\ \mu\mathrm{m}^{-1}$) and with a broadening parameter $\gamma = 0.216$ (corresponding to FWHM $\gamma\lambda_0 = 469$ Å, or $\gamma\lambda_0^{-1} = 0.992\ \mu\mathrm{m}^{-1}$). The strength of the absorption is such that on an average diffuse cloud sightline in the Milky Way, the 2175 Å profile corresponds to an oscillator strength per H nucleon $n_{\rm X} f_{\rm X}/n_{\rm H} \approx 9.3 \times 10^{-6}$ (Draine 1989a). Because we expect the oscillator strength per molecule $f_{\rm X} \lesssim 0.5$, it can be concluded that the carrier molecule must contain one or more elements from {C,O,Mg,Si,Fe}, as these are the only condensible elements with sufficiently high abundances $n_{\rm X}/n_{\rm H} \gtrsim 2 \times 10^{-5}$ in the ISM.

Fitzpatrick & Massa (1986) show that the width of the feature varies considerably from one sightline to another. The FWHM has an average value $0.992\ \mu\mathrm{m}^{-1}$, but the distribution has a $\pm 2\sigma$ variation of $\pm 12\%$. This variability in FWHM is in contrast to the fact that the central wavelength λ_0 is nearly invariant from one sightline to another: Although variations are detected, λ_0 shows $\pm 2\sigma$ variations of only $\pm 0.46\%$.

Immediately following discovery of the 2175 Å feature by Stecher (1965), Stecher & Donn (1965) pointed out that small graphite particles would produce absorption very similar to the observed feature. Although noncarbonaceous carriers have been proposed [e.g., OH^- on small silicate grains (Steel & Duley 1987)], it now seems likely that some form of graphitic carbon is responsible for the observed feature.

The C atoms in graphite are bound to one another in hexagonal sheets. Each C atom has four valence electrons ($2s^2 2p^2$); three of these are in trigonal sp^2 or

σ orbitals; the remaining electron is in a delocalized π orbital, which is shared among the C–C bonds. The individual sheets of carbon atoms are held parallel to one another only by weak van der Waals forces. Absorption of a photon can excite a π electron to an excited orbital (π^*); this $\pi \rightarrow \pi^*$ transition is responsible for the absorption feature peaking at $\sim$2175 Å. Using the dielectric function of graphite (Draine & Lee 1984), one finds that randomly oriented small graphite spheres would have an oscillator strength $f = 0.16$ per C atom (Draine 1989a). Thus, the observed 2175 Å extinction feature would require C/H $= 5.8 \times 10^{-5}$ in small graphite spheres, compatible with interstellar abundance constraints.

Although graphite is an attractive candidate, the graphite hypothesis does not appear to have a natural way to accommodate the observed variations in FWHM of the profile while at the same time holding λ_0 nearly constant: Variations in graphite grain shape and size produce variations in FWHM, but these are accompanied by changes in λ_0 (Draine & Malhotra 1993).

Mennella et al. (1998) propose that the 2175 Å feature is due to UV-processed HAC particles but do not appear to have actually measured in the lab a profile matching the interstellar 2175 Å feature.

Wada et al. (1999) propose that the 2175 Å feature is due to onion-like hyperfullerene carbon particles. Although these particles do have an absorption peak near 2200 Å, the feature appears to be broader than the interstellar profile.

The carbon atom skeleton of polycyclic aromatic hydrocarbon (PAH) molecules is very similar to a portion of a graphite sheet, with similar electronic wavefunctions. It is therefore not surprising that PAH molecules generally have strong $\pi \rightarrow \pi^*$ absorption in the 2000–2500 Å region. Thus, large PAH molecules are candidates to be the carrier of the interstellar 2175 Å feature—this is a natural extension of the graphite hypothesis.

The grain model of Weingartner & Draine (2001a) and Li & Draine (2001b) has C/H $= 6.0 \times 10^{-5}$ in PAH molecules or clusters containing from 20 to 10^5 C atoms—this population of PAH molecules is required to reproduce the observed infrared emission (see Section 9). Absorption profiles are not known for PAH molecules of the sizes characteristic of the interstellar PAHs, but one would expect a similar $\pi \rightarrow \pi^*$ oscillator strength per C as for graphite, or $f \approx 0.16$. Thus, we see that in this grain model, the 2175 Å extinction feature is expected to be primarily—perhaps entirely—due to large PAH molecules.

In this interpretation, the observed band profile would be due to a mixture of PAHs, and the observed variations in FWHM (and small variations in λ_0) would result from differences in the PAH mix from one sightline to another.

3.2. Silicate Features

The infrared extinction includes a strong absorption feature peaking at $\sim$9.7 μm. Silicate minerals generally have strong absorption resonances near 10 μm due to the Si-O stretching mode, and it seems virtually certain that the interstellar 9.7 μm feature is due to absorption by interstellar silicate material. This conclusion is strengthened by the fact that a 10 μm emission feature is observed in outflows

from cool oxygen-rich stars (which would be expected to condense silicate dust) but not in the outflows from carbon-rich stars (where silicates do not form because all of the oxygen is locked up in CO). There is also a broad feature at 18 μm that is presumed to be the O-Si-O bending mode in silicates (McCarthy et al. 1980, Smith et al. 2000).

The Trapezium (Gillett et al. 1975) emission implies $\tau(\lambda)$ with FWHM $\approx$ 3.45 μm, whereas μ Cep (Russell et al. 1975) has FWHM = 2.3 μm, so the silicate properties are not universal. On sightlines dominated by relatively diffuse clouds (e.g., toward the B5 hypergiant Cyg OB2-12 or distant WC stars) the 9.7 μm absorption appears to be better fit by the narrower μ Cep profile (Roche & Aitken 1984, Bowey et al. 1998). The silicates in molecular clouds, however, seem better fit by the broader Trapezium profile (Bowey et al. 1998).

The strength of the 9.7 μm feature relative to A_V has been measured toward Cyg OB2-12 and toward WC stars. The studies in Table 1 together indicate $A_V/\Delta\tau_{9.7} = 18.5 \pm 2.0$, where the uncertainty includes a subjective allowance for systematic errors in the model fitting.

The interstellar 9.7 μm feature is broad and relatively featureless, as opposed to absorption profiles measured in the laboratory for crystalline silicates, which show considerable structure that can be used to identify the precise mineral. The absence of substructure in the interstellar profile is believed to indicate that the interstellar silicates are largely amorphous rather than crystalline. Amorphous or glassy silicates can be produced in the laboratory by ion bombardment of initially crystalline material (Kraetschmer & Huffman 1979), formation in smokes (Day 1979), rapid quenching of a melt (Jäger et al. 1994), or deposition following evaporation (Koike & Tsuchiyama 1992, Stephens et al. 1995, Scott & Duley 1996). The laboratory profiles are in some cases quite similar to the interstellar profile, supporting the view that interstellar silicates are amorphous.

TABLE 1 Silicate 9.7 μm feature strength

Sightline	l (°)	b (°)	d (kpc)	A_V (mag)	$\Delta\tau_{9.7}$	$A_V/\Delta\tau_{9.7}$	Reference
Gal. center	0	0	8.5	34 ± 4	3.6 ± 0.3	9 ± 1	Roche & Aitken (1985)
Cyg OB2-12	80.10	0.83	1.7	10	0.58	17.2	Roche & Aitken (1984)
”				10.2	0.54	18.9	Whittet et al. (1997)
”				10.2	0.64	15.9	Bowey et al. (1998)
WR98A	358.13	−0.03	1.90	12.5	0.62	20.2	van der Hucht et al. (1996)
”				11.2	0.64	17.4	Schutte et al. (1998)
WR112	12.14	−1.19	4.15	13	0.61	21.3	Roche & Aitken (1984)
”				11.9	0.64	18.6	van der Hucht et al. (1996)
”				12.0	0.56	21.4	Schutte et al. (1998)
WR118	21.80	−0.22	3.13	13.3	0.69	19.3	Roche & Aitken (1984)
”				12.6	0.65	19.4	van der Hucht et al. (1996)
”				12.8	0.71	18.0	Schutte et al. (1998)
	Local Diffuse ISM					18.5 ± 2	overall

The observed strength per H nucleon of the interstellar silicate band appears to require that close to 100% of the solar abundance of Si, Fe, and Mg be condensed into amorphous grains. Mathis (1998) has argued that the observed strength can only be reproduced if silicate grains are "fluffy," with $\geq$25% vacuum, as in the grain model of Mathis & Whiffen (1989).

The observed 10 μm profile appears to be consistent with amorphous material with a composition in the olivine family, $Mg_{2x}Fe_{2-2x}SiO_4$. Because Mg and Fe are of approximately equal abundance in the Sun, it would be reasonable to have $x \approx 0.5$. Li & Draine (2001a) conclude that spectrophotometry of the 9.7 μm feature in extinction toward Cyg OB2-12 (Bowey et al. 1998) limits the fraction of the Si in crystalline silicates to be $\lesssim$5%. Demyk et al. (1999) find that for two protostellar objects, at most 2% of the silicates could be crystalline.

However, Bowey & Adamson (2002) argue that the observed 10 μm profile toward Cyg OB2-12 is consistent with a mixture of amorphous silicates (40% by mass) and eight crystalline pyroxenes (60% by mass); each of the crystalline species in their mix contributes $\sim$7.5% by mass, and the fine structure in the 10 μm profile appears to be consistent with the observations.

However, this interpretation raises various concerns:

- The lab measurements were for powders in a KBr matrix; spectra in vacuo would be different. Bowey & Adamson (2002) state that the "KBr shift" is minimal, but it would be expected to be significant near these strong resonances.
- A mix of crystalline grains that gives a smooth absorption profile will not give a smooth emission profile unless the different crystalline materials are heated to the same temperature.
- The different crystalline types have distinct far-infrared modes. The smoothness of the far-infrared spectra of star-forming regions places upper limits on crystalline abundances. For example, the proposed mixture has $\sim$7.5% of the Si atoms in diopside, but the observations of Onaka & Okada (2003) (see below) limit diopside to $\lesssim$2% of interstellar Si.
- It is not apparent that the proposed mixture would be consistent with the 18 μm extinction profile.
- The polarization profile of grains near strong resonances is sensitive to the dielectric function. It is not apparent that the proposed mixture would be consistent with spectropolarimetric constraints (see below).

Further study of these points is urgently required. In the text below it is assumed that interstellar silicates are predominantly amorphous, but the reader should keep in mind that a significant crystalline fraction may be possible.

The 9.7 μm and 18 μm silicate features can be observed in polarization, either in absorption or in emission. For strong resonances (such as the two silicate features), the polarization profile differs from the absorption profile, so that spectropolarimetry can constrain the dielectric function of the grain material (Martin 1975). The observed intensity and polarization across the 9.7 μm feature appear

to be approximately consistent with the "astronomical silicate" dielectric function estimated by Draine & Lee (1984), but the observed 20 μm polarization is stronger than expected for that dielectric function (Aitken et al. 1989, Smith et al. 2000).

Onaka & Okada (2003) report detection of an emission feature at 65 μm that may be due to diopside $CaMgSi_2O_6$, containing 5%–10% of interstellar Ca (corresponding to 0.35%–0.7% of interstellar Si); if confirmed, this would be the first evidence for crystalline silicates in the ISM. Although crystalline silicates are not abundant in the ISM, there is evidence from distinctive emission features for their presence in dust disks around main-sequence stars (see Artymowicz 2000, for a summary), young stellar objects and evolved stars (see Waelkens et al. 2000, for a summary), and in some solar-system comets (see Hanner 1999, for a summary), see Section 5.1 below. Nevertheless, even in these systems most of the silicate material remains amorphous.

3.3. Diffuse Interstellar Bands

The observed extinction curve includes a large number of weak extinction features, known as the diffuse interstellar bands, or DIBs. The DIBs have FWHM $\gtrsim 1$ Å, too broad to be due to molecules with $\lesssim 5$ atoms in the gas phase, and are therefore features of the grain population. Jenniskens & Désert (1994) list 154 "certain" DIBs in the interval 0.38–0.868 μm, plus an additional 52 "probable" detections. Figure 5 shows an average extinction curve for $1.5\ \mu\mathrm{m}^{-1} < \lambda^{-1} < 1.75\ \mu\mathrm{m}^{-1}$, a wavelength range that includes several strong DIBs, most notably the DIB at 5780 Å. This curve consists of the smooth extinction calculated using the Fitzpatrick (1999) parametrization plus individual diffuse bands approximated by Drude profiles with central wavelengths, FWHM, and strengths from the tabulation of Jenniskens & Désert.

The first DIBs were discovered more than 80 years ago (Heger 1922) and their interstellar nature was established 69 years ago (Merrill 1934), yet to date not a single DIB has been convincingly identified. Some of the DIBs may be absorption features produced by individual PAH molecules in the interstellar PAH mixture. Désert et al. (1995) report a positive correlation between the strength of the 2175 Å bump and the strength of certain DIBs. High-resolution observations of the 5797 Å and 6614 Å DIBs show fine structure that could be indicative of rotational bands (Kerr et al. 1996, 1998).

DIBs have recently been detected toward reddened stars in the LMC and SMC (Ehrenfreund et al. 2002).

If the DIBs were due to absorption in the aligned grains responsible for the polarization of starlight (see Section 6) there should be excess polarization associated with the DIBs (Martin & Angel 1974, Purcell & Shapiro 1977). All attempts to measure polarization structure associated with DIBs have yielded only upper limits (see Adamson & Whittet 1995) that appear to require that at least the DIBs that have been studied originate in nonaligned material, consistent with a molecular origin.

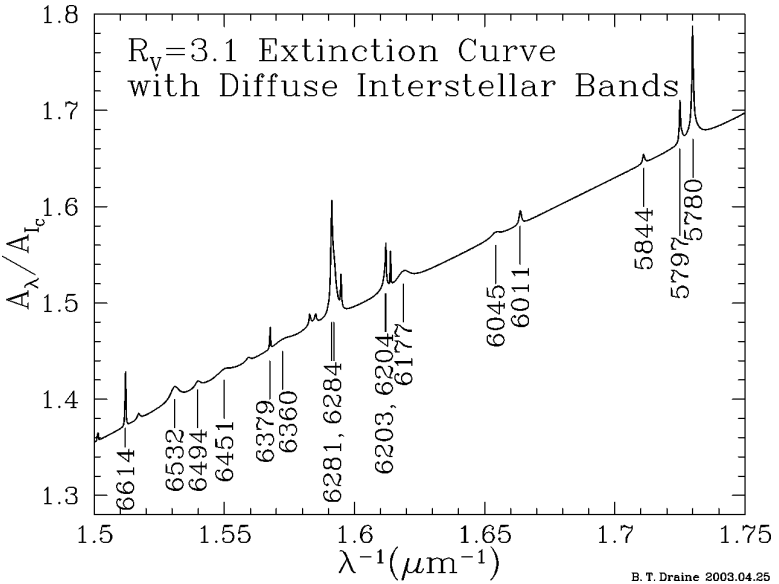

Figure 5 Diffuse interstellar bands in the 5700–6670 Å region, using DIB parameters from Jenniskens & Désert (1994).

At this time the carriers of the DIBs remain unknown, but it seems likely that at least some are due to large molecules/ultrasmall grains, possibly of PAH composition.

3.4. μm Feature: Aliphatic C-H Stretch

A broad extinction feature at 3.4 μm is measurable on sightlines with $A_V \gtrsim 10$ mag (Adamson et al. 1990). The feature appears to be present in diffuse atomic regions (in contrast to the ice features, see Section 3.5), and therefore is likely due to "refractory" grain material. The C-H stretching mode in aliphatic (chain-like) hydrocarbons occurs at 3.4 μm. Because such hydrocarbons are plausible grain constituents, the observed 3.4 μm absorption is generally attributed to the aliphatic C-H stretch (Sandford et al. 1991).

Unfortunately, aliphatic hydrocarbons show considerable variation in the C-H band strength, so it has not been possible to use the measured 3.4 μm feature to determine the abundance of aliphatic hydrocarbon material in the interstellar grain population, nor is it possible to identify the specific hydrocarbon material (Pendleton & Allamandola 2002). Sandford et al. (1991, 1995) suggest that the 3.4 μm feature in the diffuse ISM is due mainly to short saturated aliphatic chains containing $\sim$4% of the total C abundance. Greenberg et al. (1995) suggest that the 3.4 μm feature is due to carbonaceous organic residues produced by UV photolysis of ice mantles; Duley et al. (1998) attribute the feature to hydrogenated amorphous carbon (HAC) material incorporating 20%–25% of the total C abundance.

In grain models where the 3.4 μm absorption is assumed to arise in hydrocarbon mantles coating silicate grains (e.g., Li & Greenberg 1997), the 3.4 μm feature would be polarized when the 9.7 μm silicate feature is polarized; this allows a direct test of the silicate core/hydrocarbon mantle model for interstellar dust (Li & Greenberg 2002).

3.5. Ice Features

Sightlines passing through dense molecular clouds typically show additional absorption features. The strongest feature is the 3.1 μm O-H stretching mode in solid H_2O. Whittet et al. (1988) showed that in the Taurus dark cloud complex, the strength of this feature is approximately given by

$$\Delta\tau_{3.1} \approx \begin{cases} 0 & \text{for } A_V \lesssim 3.3 \text{ mag}, \\ 0.093(A_V - 3.3 \text{ mag}) & \text{for } A_V \gtrsim 3.3 \text{ mag}, \end{cases} \quad (7)$$

suggesting that dust in regions with $A_V > 3.3$ has an ice coating, whereas dust in regions with $A_V < 3.3$ is iceless. The 3.1 μm feature is accompanied by a number of weaker features due to H_2O, plus additional features due to CO_2, NH_3, CO, CH_3OH, CH_4, and other species. The features due to different species often overlap, and the positions and shapes of particular spectral features can be sensitive to the composition of the frozen mixture, complicating abundance determinations. Table 2 gives the abundances relative to H_2O estimated for two sightlines into dense star-forming regions (W33A and W3:IRS5) and for the sightline to Sgr A* at the Galactic Center. Although all three sightlines have similar CO_2/H_2O ratios, the abundances of other species (e.g., CH_3OH) vary considerably from one sightline to another. The composition of the ice mantle must be sensitive to both local environment and history.

The grains in star-forming clouds are often aligned (see Section 6.2), and the radiation reaching us from embedded sources is often polarized. Polarization has been measured in the features at 3.1 μm (H_2O), 4.6 μm (XCN), and 4.67 μm (CO) (Chrysostomou et al. 1996, Hough et al. 1996).

3.6. 3.3, 6.2, 7.7, 8.6, and 11.3 μm PAH Features

Many emission nebulae (HII regions, planetary nebulae) and reflection nebulae show emission in the 3–15 μm region that is far stronger than expected from $a \gtrsim 100$ Å grains heated by the ambient radiation field and emitting thermally. Much of the emission is concentrated in five features at 3.3, 6.2, 7.7, 8.6, and 11.3 μm (see Figure 6). Leger & Puget (1984) identified these features as the optically active vibrational modes of PAH molecules. When H atoms are attached to the edge of an aromatic ring skeleton, there are characteristic optically active vibrational modes (Allamandola et al. 1989):

- C-H stretching mode at 3.3 μm
- C-C stretching mode at 6.2 μm

TABLE 2 Major ice components

			$N(X)/N(H_2O)$		
X	**$\lambda(\mu m)$**	**$\Delta\tau_\lambda$ W33A**	**W33A**	**W3:IRS5**	**GC**
H_2O	3.1[a]	5.5 ± 0.5[b]	1	1	1
XCN	4.62	1.4[b]	.035[b]		
CO	4.67	1.3[c]	.081[c]	.030[c]	<0.12[d]
H_2CO	5.81[e]	0.17[e]	.065[e]	—	$<.024$[d]
CH_4	7.7	0.11[f]	.016[b]	.0043[f]	.024[d]
NH_3	9.0[g]		<0.05[h]	$<.035$[f]	0.2–0.3[i]
CH_3OH	9.8[j]	0.9 ± 0.2[b]	0.18[b]	$<.004$[f]	$<.04$[d]
CO_2	15.2[k]	0.58[c]	0.13[c]	0.13[c]	0.14[c]

[a]Also 6.0, 13.5, 45 μm
[b]Gibb et al. (2000)
[c]Gerakines et al. (1999)
[d]Chiar et al. (2000)
[e]Keane et al. (2001)
[f]Gürtler et al. (2002)
[g]Also 2.27, 2.96, 3.48 μm
[h]Taban et al. (2003)
[i]Lacy et al. (1998)
[j]Also 4.27 μm
[k]Also 3.53, 6.85 μm

- C-C stretching mode at 7.7 μm
- C-H in-plane bending mode at 8.6 μm
- C-H out-of-plane bending mode with wavelength depending on the number of neighboring H atoms:
  - 11.3 μm for mono H (no adjacent H)
  - 12.0 μm for duo H (2 contiguous H)
  - 12.7 μm for trio H (3 contiguous H)
  - 13.55 μm for quartet H (4 contiguous H)

Examples of mono, duo, trio, and quartet sites are indicated in Figure 7. Although the broadness of the observed features precludes identification of specific PAH molecules, a population of PAH molecules appears to provide a natural explanation for the observed emission spectrum, where the vibrational excitation is assumed to be the result of "internal conversion" of energy following absorption of an optical or UV photon (Leger & Puget 1984, Allamandola et al. 1989).

There should in principle be absorption associated with these emission features. An absorption feature at 6.2 μm (see Figure 4) has been observed (Schutte et al.

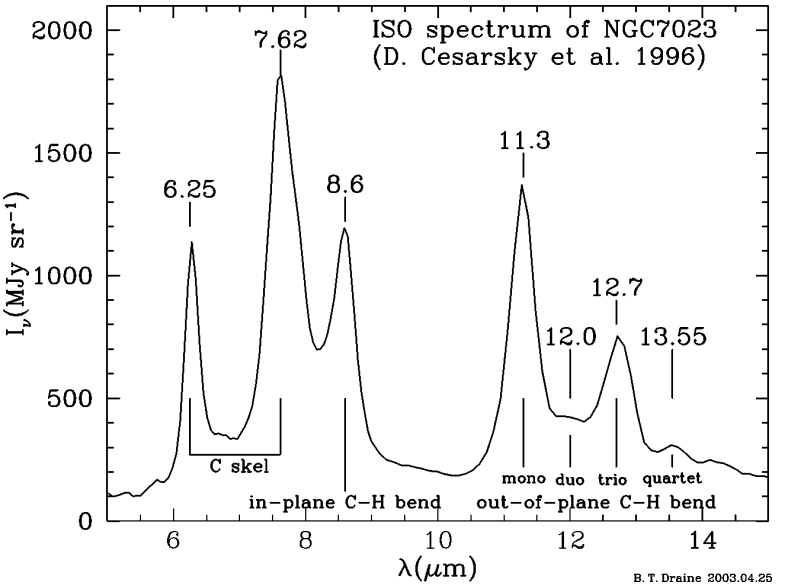

Figure 6 PAH emission features in the 5–15 μm spectrum of the reflection nebula NGC 7023.

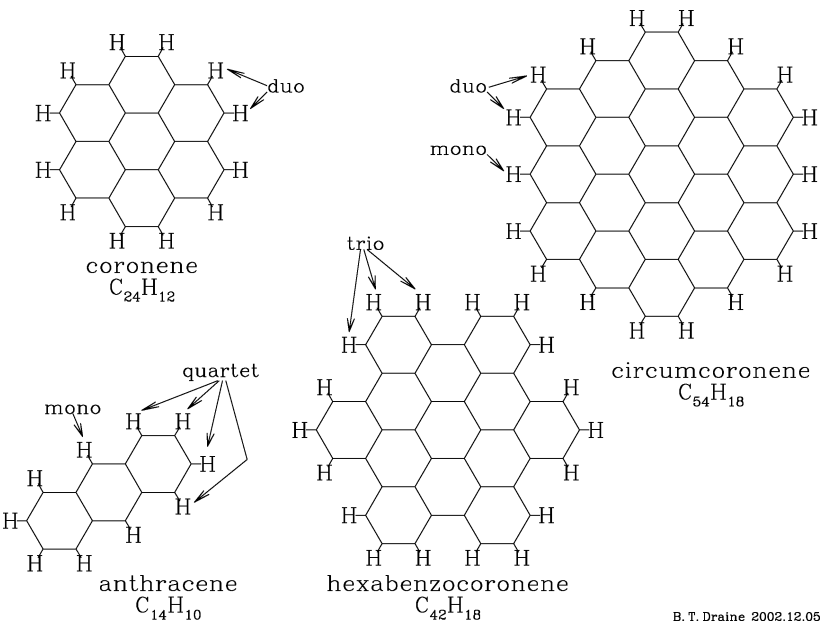

Figure 7 The structure of 4 PAH molecules. Examples of mono, duo, trio, and quartet H sites are indicated.

1998, Chiar et al. 2000). It matches closely the expected 6.2 μm absorption feature (Li & Draine 2001b).

3.7. X-Ray Absorption Edges

Interstellar grains absorb and scatter X rays. The X-ray absorption by atoms such as C, O, Mg, Si, and Fe will show photoelectric absorption edges similar to atoms in the gas phase, but the precise energy and structure of the absorption edge will be dependent on the chemical nature of the grain material (Forrey et al. 1998, Draine 2003b). Significant structure in both scattering and absorption is expected near the C K (284 eV), O K (538 eV), Fe $L_{2,3}$ (708, 721 eV), Mg K (1311 eV), Si K (1846 eV), and Fe K (7123 eV) edges (Draine 2003b). The Chandra observatory has been used to study the absorption edges of O (Paerels et al. 2001, Takei et al. 2002) and O, Mg, Si, and Fe (Schulz et al. 2002), but it has not yet proved possible to identify the chemical form in which the solid-phase Mg, Si, Fe, and O are bound.

3.8. Extended Red Emission

The extended red emission (ERE) from dust grains provides a potentially important clue to the composition of interstellar dust. The ERE consists of a broad featureless emission band between $\sim$5400 Å and $\sim$9000 Å, peaking at 6100 Å $\lesssim \lambda_p \lesssim$ 8200 Å, and with a FWHM in the range 600–1000 Å. The peak wavelength λ_p and band profile appear to vary from one region to another.

First observed in the Red Rectangle (Schmidt et al. 1980), ERE has since been seen in a wide variety of dusty environments, including reflection nebulae (Witt & Schild 1985, Witt & Boroson 1990), planetary nebulae (Furton & Witt 1990), HII regions (Darbon et al. 2000), the diffuse ISM of our Galaxy (Gordon et al. 1998, Szomoru & Guhathakurta 1998), and from other galaxies (Pierini et al. 2002).

The ERE must be photoluminescence: absorption of a starlight photon followed by emission of a lower energy photoluminescence photon. Based on the detection of ERE from the diffuse ISM, the photon conversion efficiency of interstellar dust is estimated to be $10\% \pm 3\%$ (Gordon et al. 1998, Szomoru & Guhathakurta 1998). The photoluminescence efficiency of the ERE carrier must exceed this because it is presumably not the only UV/visible photon absorber.

The luminescing substance remains uncertain. Candidate ERE materials include HAC (Duley 1985, Witt & Schild 1988), PAHs (d'Hendecourt et al. 1986), quenched carbonaceous composite (Sakata et al. 1992), C_{60} (Webster 1993), coal (Papoular et al. 1996), silicon nanoparticles (Ledoux et al. 1998, Witt et al. 1998, Smith & Witt 2002), and carbon nanoparticles (Seahra & Duley 1999).

Most candidate materials appear unable to match the observed ERE spectra and efficiency (Witt et al. 1998). Lab studies of the luminescence spectrum of hydrogenated amorphous carbon (HAC) appeared to show a good match to

observed ERE spectra (Witt & Schild 1988), provided the HAC is annealed sufficiently to shift the luminescence into the red, where it is observed; however, such red-luminescing HAC has a very low photoluminescence efficiency (Furton & Witt 1993; Rusli et al. 1996) that is incompatible with the high efficiency required to explain the ERE from the diffuse ISM.

Each of the nanoparticle hypotheses appears to have difficulties: (*a*) Seahra & Duley (1999) argue that small carbon particles with mixed sp^2/sp^3 bonding can reproduce the observed ERE profile and required efficiency, but they predict a second ERE peak at $\sim$1 μm that does not appear to be present in NGC 7023 (Gordon et al. 2000). (*b*) The PAH hypothesis has difficulty with ERE emission and PAH emission having differing spatial distributions in HII regions (Sivan & Perrin 1993; Darbon et al. 2000), and nondetection of ERE in reflection nebulae illuminated by stars with $T_{\rm eff} < 7000$ K (Darbon et al. 1999), whereas PAH emission bands are seen in these regions. (*c*) The silicon nanoparticle hypothesis appears to be ruled out by nondetection of $\sim$20 μm emission that should result from single-photon heating (see Section 9) in the silicon nanoparticle model (Li & Draine 2002a).

Recently, two new emission features have been reported in the near-infrared, at 1.15 and 1.5 μm (Gordon et al. 2000). Smith et al. (2001) propose that the 1.5 μm feature is due to β-$FeSi_2$.

Although it would appear that all current proposals have been ruled out, the arguments against them are not yet conclusive. For example, perhaps it is possible to prepare HAC samples that achieve a higher photoluminescence efficiency, or there may be some way to explain the lack of PAH emission seen in the Bubble nebula, or silicon nanoparticles might be part of larger structures. At this point it seems appropriate to continue consideration of HAC, PAHs, and silicon nanoparticles as candidate ERE carriers.

4. PRESOLAR GRAINS IN METEORITES AND INTERPLANETARY DUST

The most primitive meteorites contain presolar grains, which are recognized by virtue of isotopically anomalous composition—see Hoppe & Zinner (2000) for a recent review. Table 3 lists the six presolar grain types that have been identified thus far, along with their abundance (fraction of the total mass) in the bulk meteorite. Nanodiamond (sp^3-bonded carbon) grains make up 0.05% = 500 ppm of the meteorite. A tiny fraction of the nanodiamond particles contain a trapped Xe atom; the isotopic abundances of the trapped Xe suggests formation in SN ejecta. SiC grains are the next most abundant by mass (6 ppm), with isotopic patterns that indicate formation primarily in outflows from AGB stars. Approximately 0.5% of the SiC grains are of "Type X," with isotopic abundances, including live ^{44}Ti ($T_{1/2} = 59$ years) at the time of grain formation, which suggest formation in

TABLE 3 Presolar grains in meteorites (Hoppe & Zinner 2000)

Composition	Diameter (μm)	Abundance[a]	Origins[b]
C(diamond)	0.002	5×10^{-4}	SN
SiC[c]	0.3–20	6×10^{-6}	AGB
C(graphite)[d]	1–20	1×10^{-6}	AGB, SN II, nova
SiC type X	1–5	6×10^{-8}	SN
Al_2O_3 (corundum)	0.5–3	3×10^{-8}	RG, AGB
Si_3N_4	$\sim$1	2×10^{-9}	SN II

[a]Overall abundance in primitive carbonaceous chondrite meteorites.

[b]SN = supernova; AGB = asymptotic giant branch star; RG = red giant.

[c]SiC grains sometimes contain very small TiC inclusions.

[d]Graphite grains sometimes contain very small TiC, ZrC, and MoC inclusions.

Type II supernovae. Approximately 1 ppm of the meteorite consists of graphitic (sp^2-bonded carbon) grains, formed in AGB stars, supernovae, and novae. Al_2O_3 corundum grains are found, at least some of which appear to have formed in outflows from red giants and AGB stars. Finally, there are also Si_3N_4 grains, which appear to have a SN II origin.

It is important to recognize that the procedures used to search for presolar grains in meteorites begin with chemical treatments designed to dissolve the silicate matrix in which the presolar grains are embedded. It therefore comes as no surprise that silicates are not present in Table 3. It should also be recognized that the formation of even the most primitive meteorites involved temperatures high enough to melt rocks, in an environment that was presumably oxidizing (since the solar nebula had O/C > 1). Therefore, the relative abundances in Table 3 probably have more to do with the ability of grain types to survive a period of exposure to a hot, oxidizing environment than with interstellar abundance.

Much more informative would be the abundances of presolar grains in cometary material. A core sample would be ideal, but at this time there is no planned mission for returning a sample of pristine cometary ice to Earth. However, the Stardust mission (Brownlee et al. 2000) will collect cometary dust on an aerogel panel during the 6.1 km s^{-1} encounter of the Stardust spacecraft with Comet Wild 2 in January 2004 and return it to Earth.

Interstellar grains enter the solar system and have been detected by the Ulysses and Galileo spacecrafts; the impact rate is consistent with expectations for $a \approx 0.3\,\mu$m grains, but the impact rate for $a \gtrsim 1\,\mu$m grains is much larger than expected for the average interstellar dust distribution (Frisch et al. 1999, Weingartner & Draine 2001a). The Stardust mission will expose an aerogel panel to interstellar grains flowing through the solar system; with $\sim$25 km s^{-1} impact speeds, these grains are likely to be destroyed, but their residue in the aerogel can be analyzed for total mass and composition. We await the return of Stardust in January 2006.

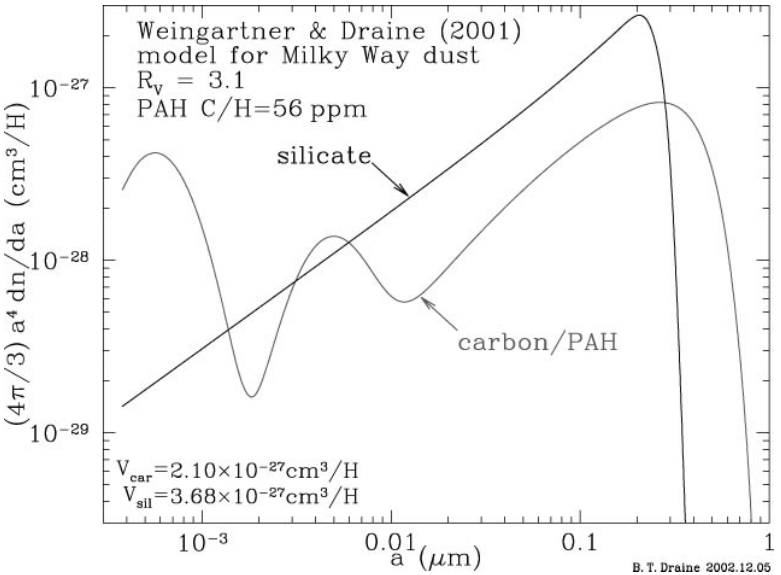

Figure 8 Size distributions for carbonaceous-silicate grain model of Weingartner & Draine (2001a) for Milky Way dust with $R_V = 3.1$, but with abundances decreased by a factor 0.93 (see text).

Active comets release their dust grains, which become part of the interplanetary dust particle (IDP) population. IDPs can be collected from the Earth's atmosphere (Brownlee 1985). Bradley (1994) identifies a class of glassy silicate IDPs, known as GEMS (Glass with Embedded Metals and Sulfides), which appear to be presolar. Most GEMS are between 0.1 and 0.5 μm in diameter—similar to the sizes of interstellar silicates (see Figure 8). The $8-13$ μm infrared absorption spectrum of these grains is similar to interstellar silicates (Bradley et al. 1999).

5. CANDIDATE GRAIN MATERIALS

Based on the observations and clues described above, it is possible to formulate a short list of candidate materials for the bulk of interstellar dust. We omit from consideration rare materials like Al_2O_3—even though Al is depleted from the gas phase, given the solar abundance of Al (Al/H $= 3.1 \times 10^{-6}$) aluminum-based materials account for only a few percent of interstellar grain mass.

5.1. Silicates

There is little doubt that silicate material contributes a substantial fraction of the total mass of interstellar dust. As discussed above (Section 3.2), in the ISM, at least $\sim$95% of the silicate material is amorphous (Li & Draine 2002a). In some

circumstellar disks the crystalline fraction appears to be higher, although it appears that the bulk of the silicates remain amorphous. Bouwman et al. (2001) find that 5%–10% of the olivine mass is crystalline in the dust around Herbig Ae/Be stars.

Cosmic abundances dictate that the dominant metal ions in silicates will be either Mg, Fe, or both. There are two general chemical classes of crystalline silicates: Mg-Fe pyroxenes $Mg_xFe_{1-x}SiO_3$ (including enstatite $MgSiO_3$ and ferrosilite $FeSiO_3$) and olivines $Mg_{2x}Fe_{2-2x}SiO_4$ (including forsterite Mg_2SiO_4 and fayalite Fe_2SiO_4). There are two different crystalline structures for the pyroxenes: orthopyroxene and clinopyroxene.

The optical constants of various crystalline pyroxenes have been measured by Jäger et al. (1998) and Chihara et al. (2002); crystalline olivines have been measured by Jäger et al. (1998), Koike et al. (1999), and Suto et al. (2002).

As noted above, some circumstellar dust exhibits emission features characteristic of crystalline silicates, and from the locations and strengths of these features it is possible to infer the Mg:Fe ratio. In all cases thus far the crystalline silicate material appears to be very Mg-rich and Fe-poor, consistent with pure forsterite and enstatite (Tielens et al. 1998, Molster et al. 2002a). Molster et al. (2002b) report that enstatite $MgSiO_3$ is more abundant than forsterite Mg_2SiO_4 around most evolved stars.

Si is generally heavily depleted in the ISM. If Si is predominantly in silicates, and if Fe is not present in silicates, then the interstellar silicates would be expected to be enstatite $MgSiO_3$. The Fe would then presumably be in either metallic Fe or in oxide form (FeO, Fe_2O_3, Fe_3O_4). However, although there is evidence for Mg-rich silicate in circumstellar dust, we do not yet have a reliable indication of the composition of interstellar silicates, so an appreciable Fe fraction and olivine-like composition are not ruled out.

Observed gas-phase abundances of Mg, Fe, and Si, and variations in these abundances from one cloud to another, have been interpreted as indicating that silicate grains may have a Mg-rich mantle and Fe-rich core (Spitzer & Fitzpatrick 1993). The total ratio of (Fe+Mg) atoms to Si atoms in grains is estimated to be $\sim$3.4:1 (Fitzpatrick 1997), $\sim$3:1 (Howk et al. 1999)—in excess of the 2:1 ratio expected for olivines, suggesting that metal oxides or metallic Fe may be present in addition to silicates. However, these conclusions depend on assumed values of the total interstellar abundances; Sofia & Meyer (2001) conclude that the (Fe+Mg):Si ratio in interstellar dust is actually close to 2:1 for both halo dust and the dust in the well-studied ζ Oph cloud.

The composition of interstellar silicates remains uncertain, but the study by Sofia & Meyer (2001) suggests that olivine $MgFeSiO_4$ appears to be a reasonable approximation.

5.2. Carbonaceous Materials

By "carbonaceous" we mean materials that are predominantly C by mass, including the following:

- diamond: sp^3-bonded carbon.
- graphite: sp^2-bonded carbon, either monocrystalline or polycrystalline.
- amorphous or glassy carbon: a mixture of sp^2- and sp^3-bonded carbon, with only short-range order.
- hydrogenated amorphous carbon: amorphous carbon with an appreciable hydrogen fraction.
- PAH: sp^2-bonded carbon with peripheral H (see Section 3.6).
- aliphatic (chainlike) hydrocarbons (see Section 3.4).

The presence of sp^2-bonded carbon is indicated by the 2175 Å feature and the PAH emission bands. The 2175 Å feature requires sp^2-bonded carbon in small ($a \lesssim 100$ Å) particles (in larger particles the 2175 Å feature is suppressed), and single-photon excitation of the PAH emission features requires very small particles, with $\lesssim 10^4$ C atoms. A PAH population incorporating a C abundance C/H $\approx 60 \times 10^{-6}$ appears able to account for both the PAH emission features (see Section 3.6) and the 2175 Å feature (see Section 3.1).

5.3. SiC

SiC grains are found in meteorites (see Section 4), and an emission feature at 11.3 μm is observed in the spectra of many carbon stars (Treffers & Cohen 1974; Blanco et al. 1998). However, absence of the 11.3 μm feature in the interstellar extinction indicates that the abundance of Si in SiC dust is less than 5% of the abundance of Si in silicates (Whittet et al. 1990). Accordingly, SiC grains, although undoubtedly present in the ISM, are not a major component of the interstellar grain mix.

5.4. Carbonates

Calcite $CaCO_3$ and dolomite $CaMg(CO_3)_2$ have been detected in dusty disks within the planetary nebulae NGC6302 and NGC6537 (Kemper et al. 2002), but these carbonates are estimated to contribute less than 1% of the dust mass. Carbonates are evidently not a major component of the interstellar grain mix.

6. POLARIZATION

6.1. Optical-UV Polarization

Light reaching us from reddened stars is often linearly polarized because the extinction depends on the polarization mode. The degree of polarization as a function of wavelength can be approximated by the "Serkowski law," a 3-parameter empirical fitting function (Serkowski 1973):

$$p(\lambda) = p_{\max} \exp\left[-K(\ln(\lambda/\lambda_{\max}))^2\right], \quad (8)$$

where $\lambda_{max} \approx 5500$ Å and $K \approx 1$ on typical sightlines through diffuse clouds. The polarization arises from differential extinction by aligned dust grains and will depend on the degree of alignment with the local magnetic field, the angle between the local magnetic field and the line of sight, and the degree to which the direction of the magnetic field varies along the line of sight. Studies of many sightlines (Serkowski et al. 1975) find that

$$p_{max} \lesssim 0.03 A(\lambda_{max})/\mathrm{mag}, \tag{9}$$

where $A(\lambda)$ is the (polarization-averaged) extinction at wavelength λ. Interstellar dust grains must be sufficiently nonspherical and sufficiently aligned so that at λ_{max} one polarization mode is extincted ~6% more than the other polarization mode. Values of $p_{max}/A(\lambda_{max}) < 0.03/\mathrm{mag}$ are presumed to result when the magnetic field is disordered or not transverse to the line of sight or from regions where the degree of grain alignment is lower.

The wavelength λ_{max} varies from one sightline to another and is correlated with the value of R_V, with

$$R_V \approx 3.67(\lambda_{max}/5500\,\text{Å}) - 0.29 \tag{10}$$

(Clayton & Mathis 1988), and

$$K \approx 1.02(\lambda_{max}/5500\,\text{Å}) - 0.10 \tag{11}$$

(Wilking et al. 1982). The Serkowski law provides quite a good fit to the data for $0.8\ \mu\mathrm{m}^{-1} \lesssim \lambda^{-1} \lesssim 3\ \mu\mathrm{m}^{-1}$. Observations in the vacuum UV (Anderson et al. 1996, Clayton et al. 1996, Wolff et al. 1997) show that the degree of polarization continues to decline with decreasing wavelength. This implies that the small grains responsible for the rising extinction in the vacuum UV are inefficient polarizers—they are either nearly spherical or minimally aligned (Kim & Martin 1995).

Most stars show no polarization excess in the 2175 Å feature but two do: A 2175 Å polarization feature is detected in HD 197770 and HD 147933-4 (Wolff et al. 1997).

6.2. Polarized Far-Infrared Emission

The aligned dust grains that polarize starlight will also produce linearly polarized infrared emission because for an isotropic dielectric function a submicron grain will radiate most effectively when the E field is parallel to the long axis of the grain. It is now possible to map this polarized emission from dense regions. For example, the W51 star-forming region has been mapped at 100 μm (Dotson et al. 2000), 850 μm (Chrysostomou et al. 2002), and 1.3 mm (Lai et al. 2001), with linear polarizations as large as 10% observed at 1.3 mm.

Hildebrand et al. (1999) have discussed the wavelength dependence of the measured polarization for dense cloud cores and envelopes. The data suggest that the grain alignment is larger in warmer regions.

Observations of quiescent clouds are consistent with no grain alignment in the central regions (Goodman et al. 1995, Padoan et al. 2001).

Radiative torques due to anisotropic starlight play an important role in the process of grain alignment (Draine & Weingartner 1997). These torques would be ineffective in the central regions of quiescent dark clouds where external starlight is heavily attenuated. In star-forming clouds such as M17 or W51, however, starlight is provided within the clouds by recently formed stars.

7. A PROVISIONAL GRAIN MODEL

Although we have quite good observational determinations of the extinction in the near-infrared, optical, and UV regions, the extinction and scattering properties of interstellar grains at very short wavelengths and very long wavelengths are probably best obtained by calculating them using a physical grain model that has been constrained by a variety of observations, including observations of extinction and infrared emission.

Mathis et al. (1977) discovered that the average interstellar extinction could be satisfactorily reproduced by a grain model containing two components—graphite grains and silicate grains. Remarkably, the extinction curve was reproduced very well if both grain components had power-law size distributions, $dn/da \propto a^{-3.5}$, truncated at a minimum size $a_- \approx 50$ Å and a maximum size $a_+ \approx 2500$ Å. The success of this grain model led Draine & Lee (1984) to refine the optical constants, and extend the treatment into the mid- and far-infrared. The graphite-silicate model was applied in the X-ray region by Laor & Draine (1993).

At the time when the graphite-silicate model was developed, PAHs had not been recognized as a major interstellar grain material. With the recognition that the interstellar grain population appears to include a substantial population of ultrasmall grains with PAH composition, the graphite-silicate model has recently been extended in a very natural way: The carbonaceous grains are now assumed to be PAH molecules when very small, but to have physical and chemical properties that can be approximated by grains of bulk graphite when larger than $\sim$0.01 μm (containing $N \gtrsim 10^6$ C atoms). The properties of the carbonaceous grains are taken to change smoothly from PAH-like to graphite-like as the grain size is increased.

Models developed to account for the infrared emission spectrum of interstellar dust require that the PAH population contain $\sim$15% of the interstellar C abundance. These particles necessarily make a major contribution to the UV extinction. Weingartner & Draine (2001a) have found size distributions for the grains that, including the PAHs, are consistent with the extinction produced by the interstellar grain population, and with the size distribution of the PAHs adjusted to reproduce the observed infrared emission from the diffuse ISM (Li & Draine 2001b).

The grain size distribution adopted by Weingartner & Draine (2001a) for average Milky Way dust (with $R_V = 3.1$) is shown in Figure 8 but with abundances reduced by a factor 0.93 to reproduce $A_{I_C}/N_{\rm H}$ from Equation 4. The carbonaceous

grain distribution is trimodal: The peak at $a \approx 0.3$ μm is required to reproduce the observed extinction curve; the peak at $a \approx .0005$ μm is required to reproduce the 3−12 μm PAH emission features; and the peak at $a \approx 0.005$ μm improves the fit to the observed emission near 60 μm. The peaks at $\sim$0.3 μm and $\sim$.0005 μm are certainly real, but the peak at $\sim$.005 μm could be an artifact of errors in the adopted grain optical and FIR cross sections.

The dielectric functions of graphite and "astrosilicate" (including structure at X-ray absorption edges) have been reestimated by Draine (2003b). The extinction and scattering cross sections per H nucleon, calculated for the Weingartner & Draine (2001a) grain model, are shown in Figures 9 and 10. For $\lambda \gtrsim 20$ μm, the extinction calculated for this grain model can be approximated by $\tau/N_{\rm H} \approx 5 \times 10^{-25}\,{\rm cm}^2(\lambda/\mu{\rm m})^{-2}$, as seen in Figure 10. The scattering varies as expected for Rayleigh scattering for $\lambda \gtrsim 4$ μm: $\tau_{\rm sca}/N_{\rm H} \approx 1.0 \times 10^{-21}\,{\rm cm}^2(\lambda/\mu{\rm m})^{-4}$.

This provisional dust model does not include a component to reproduce the observed 3.4 μm absorption feature (see Section 3.4). If the graphite in the $a \gtrsim 200$ Å carbonaceous grains is replaced with a mixture of graphite and aliphatic hydrocarbons, it seems likely that the extinction curve, including the 3.4 μm feature, could be reproduced with only slight adjustments to the grain size distribution.

The Weingartner & Draine (2001a) model has $A_V/\Delta\tau_{9.7} = 14.2$ (see Tables 4–6), 25% smaller than the observed value 18.5 for diffuse cloud dust (see Table 1)

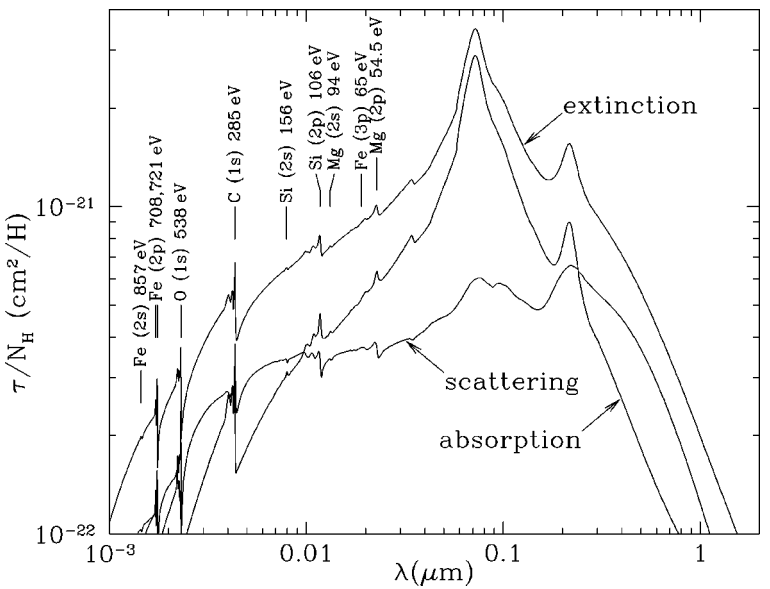

Figure 9 Extinction and scattering calculated for Weingartner & Draine (2001a) model for $R_V = 3.1$ Milky Way dust, but with abundances reduced by factor 0.93 (see text).

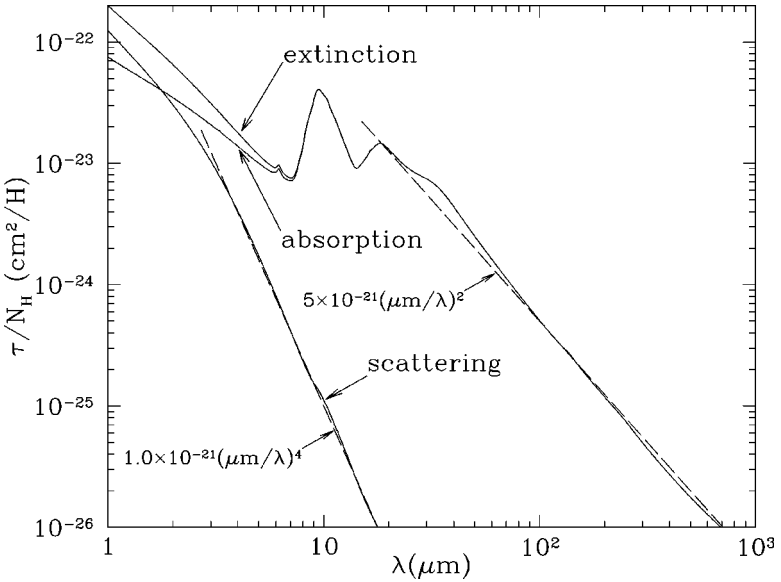

Figure 10 Extinction and scattering calculated for Weingartner & Draine (2001a) model for $R_V = 3.1$ Milky Way dust, but with abundances reduced by factor 0.93 (see text). The *dashed lines* show the asymptotic behavior of the absorption ($\propto\lambda^{-2}$) and scattering ($\propto\lambda^{-4}$) cross sections.

Evidently, the silicate abundance or the silicate band strength should be reduced by $\sim$30%.

8. SCATTERING

8.1. Optical and UV

Observations of light reflected from dust grains provides another test of dust grain models. Individual reflection nebulae are bright, but comparisons with models are uncertain because the scattering geometry is in general poorly determined: The illuminating star could be in front of the dust cloud (in which case the typical scattering angle would be large), or it could be embedded within it (in which case forward scattering by the dust grains between us and the star would dominate).

The diffuse galactic light (DGL) consists of starlight scattered off the dust in the diffuse ISM, illuminated by the general interstellar starlight radiation field. Because we think we have independent knowledge of the spatial distribution of both stars and dust, studies of dust properties using the DGL do not suffer from geometric ambiguity. However, the DGL is faint (and must be distinguished from

TABLE 4 Absorption and scattering for $5\ \mu\mathrm{m} > \lambda > 0.1\ \mu\mathrm{m}$[a]

λ		CCM89[b]	F99[c]	Model[d]				
μm	Band[e]	A_λ/A_{I_C}	A_λ/A_{I_C}	A_λ/A_{I_C}	Albedo	$\langle\cos\theta\rangle$	$C_{\rm ext}$[f] cm^2/H	$\kappa_{\rm abs}$ cm^2/g
4.750	M		.0619	.0456	0.164	−.041	1.29×10^{-23}	5.76×10^{2}
3.800	L'		.0866	.0700	0.245	−.013	1.97×10^{-23}	7.97×10^{2}
3.450	L	.0931	0.103	.0845	0.282	.006	2.38×10^{-23}	9.16×10^{2}
2.190	K	0.190	0.212	0.197	0.439	0.131	5.56×10^{-23}	1.67×10^{3}
1.630	H	0.304	0.321	0.324	0.520	0.209	9.15×10^{-23}	2.35×10^{3}
1.220	J	0.485	0.489	0.514	0.585	0.289	1.45×10^{-22}	3.22×10^{3}
1.000		0.682	0.668	0.707	0.623	0.363	1.99×10^{-22}	4.02×10^{3}
0.9000		0.792	0.819	0.836	0.642	0.401	2.36×10^{-22}	4.53×10^{3}
0.8930	z	0.803	0.830	0.847	0.643	0.404	2.39×10^{-22}	4.57×10^{3}
0.8655	I_J	0.855	0.879	0.889	0.647	0.414	2.51×10^{-22}	4.73×10^{3}
0.8020	I_C	1.000	1.000	1.000	0.658	0.438	2.82×10^{-22}	5.17×10^{3}
0.7480	i	1.134	1.125	1.111	0.665	0.459	3.13×10^{-22}	5.62×10^{3}
0.7000		1.246	1.255	1.226	0.671	0.479	3.46×10^{-22}	6.09×10^{3}
0.6492	R_C	1.365	1.419	1.368	0.674	0.500	3.86×10^{-22}	6.72×10^{3}
0.6415	R_J	1.381	1.442	1.391	0.675	0.503	3.92×10^{-22}	6.83×10^{3}
0.6165	r	1.443	1.531	1.472	0.676	0.513	4.15×10^{-22}	7.21×10^{3}
0.5470	V	1.665	1.805	1.735	0.674	0.538	4.89×10^{-22}	8.55×10^{3}
0.4685	g	2.045	2.238	2.114	0.661	0.560	5.96×10^{-22}	1.08×10^{4}
0.4405	B	2.187	2.396	2.273	0.653	0.565	6.41×10^{-22}	1.19×10^{4}
0.3635	U	2.550	2.813	2.847	0.616	0.569	8.03×10^{-22}	1.65×10^{4}
0.3550	u	2.612	2.866	2.847	0.616	0.569	8.03×10^{-22}	1.65×10^{4}
0.3000		3.005	3.306	3.328	0.582	0.556	9.38×10^{-22}	2.10×10^{4}
0.2500		3.826	4.163	4.150	0.530	0.542	1.17×10^{-21}	2.95×10^{4}
0.2300		4.729	5.115	5.052	0.459	0.545	1.42×10^{-21}	4.12×10^{4}
0.2200		5.209	5.584	5.478	0.428	0.551	1.54×10^{-21}	4.73×10^{4}
0.2175		5.264	5.626	5.515	0.424	0.554	1.56×10^{-21}	4.79×10^{4}
0.2150		5.277	5.624	5.507	0.423	0.557	1.55×10^{-21}	4.80×10^{4}
0.2100		5.173	5.503	5.381	0.428	0.563	1.52×10^{-21}	4.64×10^{4}
0.2000		4.698	5.052	4.926	0.452	0.576	1.39×10^{-21}	4.07×10^{4}
0.1900		4.322	4.705	4.542	0.466	0.594	1.28×10^{-21}	3.66×10^{4}
0.1800		4.164	4.546	4.340	0.457	0.614	1.22×10^{-21}	3.56×10^{4}
0.1600		4.232	4.585	4.346	0.403	0.653	1.23×10^{-21}	3.92×10^{4}
0.1400		4.692	5.057	4.838	0.360	0.678	1.36×10^{-21}	4.67×10^{4}
0.1200		5.928	6.234	5.787	0.321	0.675	1.63×10^{-21}	5.93×10^{4}
0.1000				7.492	0.273	0.649	2.11×10^{-21}	8.23×10^{4}

[a]Tabulated data are available at http://www.astro.princeton.edu/ ∼draine/dust/dust.html

[b]Cardelli et al. (1989) extinction fit for $R_V = 3.1$

[c]Fitzpatrick (1999) extinction fit for $R_V = 3.1$

[d]$R_V = 3.1$ Milky Way dust model of Weingartner & Draine (2001a) but with abundances reduced by 0.93, and using optical constants from Draine (2003b).

[e]$\lambda_{\rm eff}$ for $JHKLL'M$ from Bessel & Brett (1988); $R_J I_J$ from Johnson (1965); Cousins $UBVR_C I_C$ from Fukugita et al. (1996); SDSS *ugriz* from Gunn (2002, private communication).

[f]$A_\lambda = (2.5/\ln 10)C_{\rm ext}(\lambda)N_{\rm H} = 1.086 C_{\rm ext}(\lambda)N_{\rm H}$

[g]$\kappa_{\rm abs}(\lambda)$ = absorption cross section per unit dust mass. For this model, $M_{\rm H}/M_{\rm dust} = 90$.

TABLE 5 Absorption and scattering[a] for $\lambda > 5\mu$m

λ μm	A_λ/A_{I_C} model	albedo	$\langle\cos(\theta)\rangle$	C^{a}_{ext} cm^2/H	κ^{a}_{abs} cm^2/g
1000	.00002	.00000	−.004	5.48×10^{-27}	2.94×10^{-1}
850.0	.00003	.00000	−.005	7.15×10^{-27}	3.83×10^{-1}
350.0	.00013	.00000	−.005	3.58×10^{-26}	1.92×10^{0}
200.0	.00042	.00001	−.004	1.19×10^{-25}	6.37×10^{0}
140.0	.00092	.00001	.000	2.59×10^{-25}	1.39×10^{1}
100.0	.00180	.00003	.007	5.07×10^{-25}	2.71×10^{1}
60.00	.0058	.00007	.000	1.62×10^{-24}	8.70×10^{1}
40.00	.0156	.00014	−.016	4.40×10^{-24}	2.36×10^{2}
25.00	.0317	.00031	−.025	8.95×10^{-24}	4.79×10^{2}
18.00	.0514	.00066	−.026	1.45×10^{-23}	7.76×10^{2}
14.00	.0327	.00283	−.029	9.22×10^{-24}	4.92×10^{2}
12.00	.0622	.00301	−.029	1.75×10^{-23}	9.37×10^{2}
9.700	0.140	.003	−.036	3.94×10^{-23}	2.10×10^{3}
8.000	.0491	.017	−.050	1.38×10^{-23}	7.29×10^{2}
7.000	.0270	.055	−.053	7.60×10^{-24}	3.85×10^{2}
6.000	.0329	.088	−.052	9.27×10^{-24}	4.53×10^{2}

[a]See Table 4

the direct light from faint stars), and attempts to infer the grain albedo and scattering asymmetry factor $g \equiv \langle\cos\theta\rangle$ often find that there can be a one-parameter family of (albedo, g) values that are consistent with the observations.

Figures 11 and 12 show various observational estimates of albedo and g as a function of wavelength for interstellar dust, based on observations of the DGL. Determination of grain scattering properties in the reflection nebulae NGC 7023 (Witt et al. 1992), IC435 (Calzetti et al. 1995), NGC 2023 (Burgh et al. 2002), and the Pleiades (Gibson & Nordsieck 2003) are also shown.

1. There does appear to be evidence for a decrease in albedo from the optical to the vacuum UV, although the results for NGC 7023 and IC435 at $\lambda^{-1} > 5\ \mu\text{m}^{-1}$ do not conform.
2. The data are consistent with (but do not require) a rise in the scattering asymmetry factor g from optical to UV.
3. The data in Figures 11 and 12 appear to be consistent with the albedo and g calculated for the carbonaceous-silicate grain model.

The scatter in the results of different studies [e.g., the albedo and g near $\lambda \approx 1600$ Å ($\lambda^{-1} \approx 6.25\ \mu\text{m}^{-1}$) in Figures 11 and 12] serves as a warning that determining

TABLE 6 Absorption and scattering[a] for $\lambda < 0.1\ \mu$m

λ μm	$h\nu$ eV	A_λ/A_{I_C} model	Albedo	$\langle\cos(\theta)\rangle$	C_{ext}[a] cm^2/H	κ^a_{abs} cm^2/g
.09120	13.6	8.256	0.248	0.658	2.33×10^{-21}	9.37×10^4
.04881	25.4	5.574	0.291	0.813	1.57×10^{-21}	5.97×10^4
.02339	53.0	3.355	0.366	0.953	9.46×10^{-22}	3.21×10^4
.02279	54.4	3.577	0.369	0.949	1.01×10^{-21}	3.41×10^4
.02214	56.0	3.469	0.393	0.950	9.78×10^{-22}	3.18×10^4
.01240	100	2.564	0.452	0.988	7.23×10^{-22}	2.12×10^4
.01170	106	2.908	0.432	0.985	8.20×10^{-22}	2.49×10^4
.006199	200	2.000	0.578	0.997	5.64×10^{-22}	1.27×10^4
.004397	282	1.426	0.619	0.999	4.02×10^{-22}	8.20×10^3
.004350	285	2.355	0.452	0.998	6.64×10^{-22}	1.95×10^4
.004133	300	1.812	0.517	0.999	5.11×10^{-22}	1.32×10^4
.002480	500	0.971	0.632	1.000	2.74×10^{-22}	5.40×10^3
.002317	535	0.691	0.386	1.000	1.95×10^{-22}	6.40×10^3
.002305	538	1.325	0.355	1.000	3.74×10^{-22}	1.29×10^4
.002296	540	1.138	0.453	1.000	3.21×10^{-22}	9.40×10^3
.002254	550	1.056	0.478	1.000	2.98×10^{-22}	8.32×10^3
.001759	705	0.575	0.433	1.000	1.62×10^{-22}	4.92×10^3
.001751	708	1.219	0.353	1.000	3.44×10^{-22}	1.19×10^4
.001734	715	0.799	0.515	1.000	2.25×10^{-22}	5.84×10^3
.001720	721	0.941	0.432	1.000	2.65×10^{-22}	8.07×10^3
.001710	725	0.845	0.503	1.000	2.38×10^{-22}	6.33×10^3
.001550	800	0.751	0.514	1.000	2.12×10^{-22}	5.51×10^3
.001240	1000	0.563	0.564	1.000	1.59×10^{-22}	3.71×10^3
.000620	2000	0.181	0.584	1.000	5.10×10^{-23}	1.14×10^3

[a]See Table 4

the albedo is model-dependent, requires accurate photometry, and in the case of photodissociation regions like NGC 7023, NGC 2023, or IC 435, may require subtraction of fluorescent emission from H_2.

8.2. X-Ray Scattering

Interstellar grains scatter X rays through small scattering angles, and as a result X-ray point sources can appear to be surrounded by a diffuse halo of X rays scattered by dust grains between us and the source (Overbeck 1965, Hayakawa 1970, Martin 1970). Measurements of such halos provide a quantitative test of

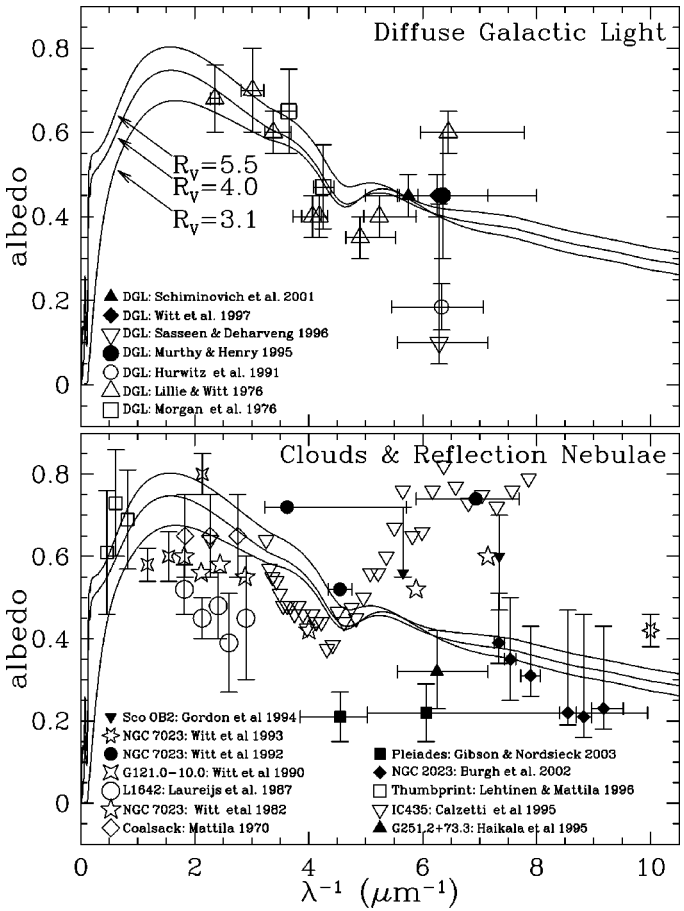

Figure 11 Solid lines: scattering albedo calculated for Weingartner & Draine (2001a) model for Milky Way dust with $R_V = 3.1$, 4.0, and 5.5. Symbols: observational determinations. After Draine (2003b).

interstellar grain models (Catura 1983, Mauche & Gorenstein 1986, Mitsuda et al. 1990, Mathis & Lee 1991, Clark et al. 1994, Woo et al. 1994, Mathis et al. 1995, Predehl & Klose 1996, Smith & Dwek 1998, Witt et al. 2001, Smith et al. 2002). Unfortunately, many of the observational studies appear to be compromised by inability to separate the scattered photons from the psf at small halo angles (see Draine 2003b).

ROSAT observations of Nova Cygni 1992 provide the best observational data at this time. Mathis et al. (1995) concluded that the observed halo on day 291 (after optical maximum) was best explained if the larger ($a \geq 0.1\ \mu$m) interstellar grains had a "fluffy" morphology, with a void fraction $\geq$25%—if the grains were compact the scattering halo would be stronger than observed. Smith & Dwek

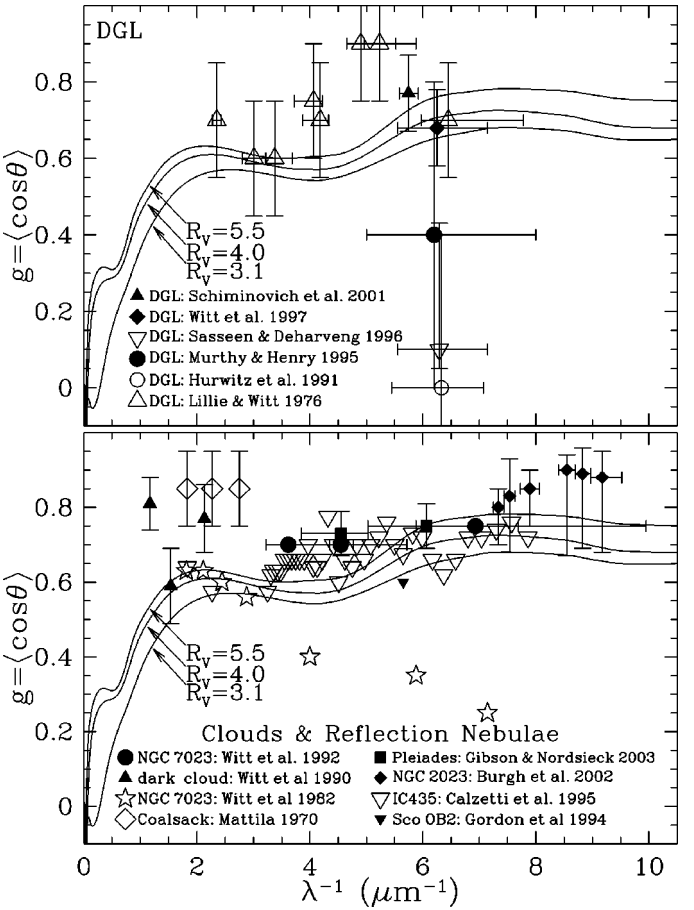

Figure 12 Solid lines: Scattering asymmetry factor $g = \langle\cos\theta\rangle$ calculated for Weingartner & Draine (2001a) model for Milky Way dust with $R_V = 3.1$, 4.0, and 5.5. Symbols: observational determinations. After Draine (2003b).

(1998) argued that Mathis et al. (1995) had overestimated the scattering due to their use of the Rayleigh-Gans approximation and that in fact the observed X-ray halo was consistent with compact grains. The same data were reconsidered by Witt et al. (2001), who concluded that the observed halo intensity at small scattering angles required a substantial population of large ($a \geq 1\ \mu$m) grains.

Draine & Tan (2003) have revisited this question. Using data for nine epochs, they find that the Weingartner & Draine (2001a) PAH/graphite/silicate grain model—with no adjustment to the size distribution—is consistent with the observed X-ray halo, for 50″–3000″ halo angles. Observations with ROSAT and Chandra of other sources at energies between 0.7 and 4 keV also appear to be

in general agreement with the scattering expected for this grain model (Draine, 2003b).

9. INFRARED EMISSION

Heating of interstellar dust grains is primarily by absorption of starlight (collisional heating dominates only in dense regions in dark clouds—where the starlight intensity has been severely attenuated—or in dense, hot, shocked gas). Because the heating by starlight photons is quantized and stochastic, the temperature of a dust grain is time dependent. Figure 13 shows the temperature histories of four dust grains heated by the average starlight background and cooled by emission of infrared photons over a time span of approximately 1 day. It is apparent that for grains heated by the average starlight background, grains with radii $a \gtrsim 200$ Å can be approximated as having a steady temperature. Grains with radii $a \lesssim 50$ Å, however, undergo very large temperature excursions, and the notion of "average temperature" is not applicable. Most of the infrared power radiated by such small grains occurs during brief intervals following photon arrivals, when the grain temperature is close to the peak.

In order to calculate the time-averaged emission spectrum for such small grains, one must calculate the energy distribution function *dP/dE* for grains of a particular

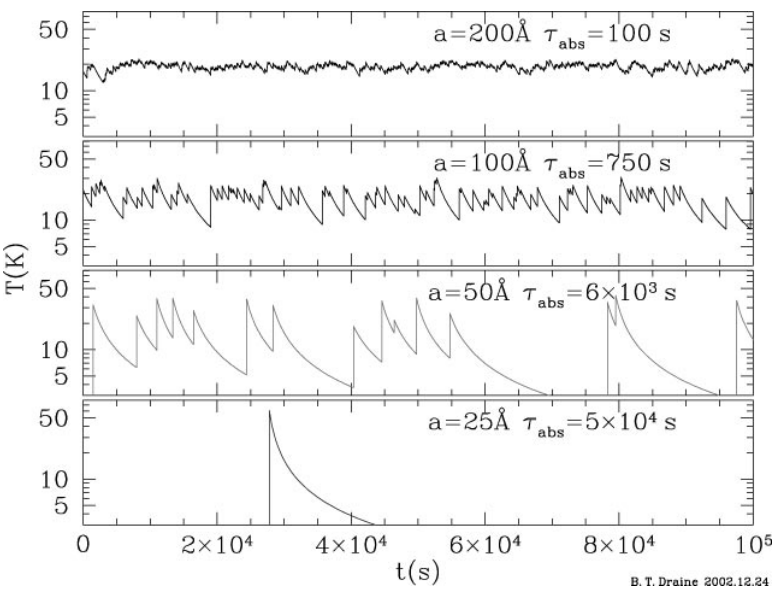

Figure 13 A day in the life of four carbonaceous grains, heated by the local interstellar radiation field. τ_{abs} is the mean time between photon absorptions (Draine & Li 2001).

size, where dP is the probability that a grain will have vibrational energy in interval $(E, E + dE)$. To solve for dP/dE, one must first calculate the specific heat for the grain, and the cross sections for absorption and emission of photons. Monte-Carlo simulations can be used to obtain dP/dE, but it is more efficient to solve for the steady-state dP/dE (Guhathakurta & Draine 1989, Draine & Li 2001).

The notion of "temperature" is somewhat problematic for very small grains, but one can define the instantaneous vibrational temperature as being equal to the temperature $T(E)$ at which the expectation value of the energy would be equal to the actual grain energy; this is the temperature plotted in Figure 13. Draine & Li (2001) have shown that a thermal estimate for the grain emissivity is a good approximation, even for grains containing as few as $\sim$30 atoms.

The infrared and far-infrared glow from interstellar dust can be measured, and a dust model must be able to reproduce the observed intensity and spectrum. The diffuse ISM at galactic latitudes $|b| \gtrsim 20^\circ$ provides a particularly clean test because we have good estimates for the intensity of the starlight heating the dust, and the observed 21 cm emission provides accurate gas column densities, which, for an assumed dust-to-gas ratio, determine the column density of dust. Although the surface brightness of the infrared emission is low, it has been detected by IRAS and COBE after averaging over large areas of sky. Figure 14 shows the observed emissivity per H nucleon, based on COBE-FIRAS and COBE-DIRBE photometry.

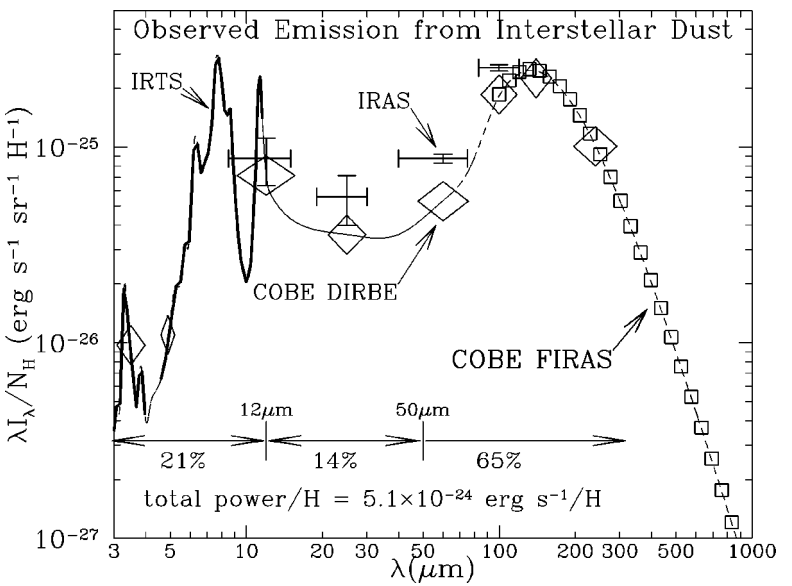

Figure 14 Observed emission from diffuse interstellar dust. *Crosses*: IRAS (Boulanger & Perault 1988); Squares: COBE-FIRAS (Finkbeiner et al. 1999); Diamonds: COBE-DIRBE (Arendt et al. 1998); Heavy Curve: IRTS (Onaka et al. 1996, Tanaka et al. 1996). The total power $\sim 5.1 \times 10^{-24}$ erg s^{-1}/H is estimated from the interpolated broken line.

3.0–4.5 μm and 4.5–11.3 μm spectra, measured at $b \approx 0$ by the IRTS satellite have been added to the plot, normalized to agree with the DIRBE photometry in the 3.5, 5.0, and 12 μm bands.

In this dust model, approximately 20% of the absorbed starlight energy is reradiated at $\lambda < 12$ μm by PAHs. The same grain model, applied to reflection nebulae, can acount for the observed dependence of dust emission spectrum on temperature of illuminating star (Li & Draine 2002b). With appropriate changes to the grain mixture, the model can also account for the observed IR emission from the SMC (Li & Draine 2002c).

Approximately two thirds of the radiated power is at $\lambda \gtrsim 50$ μm—this is emission from $a \gtrsim .01$ μm grains that are maintained at a nearly steady temperature $\sim$15$-$20 K by starlight. The remaining $\sim$one third of the radiated power is from grains with radii $a \lesssim 50$ Å that are cooling following temperature spikes resulting from absorption of individual starlight photons. We can immediately see the following: (*a*) The grain population must contain enough $a \lesssim 50$ Å grains to account for $\sim$one third of the absorption of starlight. (*b*) The resemblance of the 3–12 μm emission spectrum from the diffuse ISM to the emission spectrum expected from PAH molecules, radicals, and ions implies that a large fraction of the smallest grains must be PAHs. Figure 15 shows the emission calculated for the PAH/carbon/silicate dust model illuminated by the average interstellar radiation field spectrum.

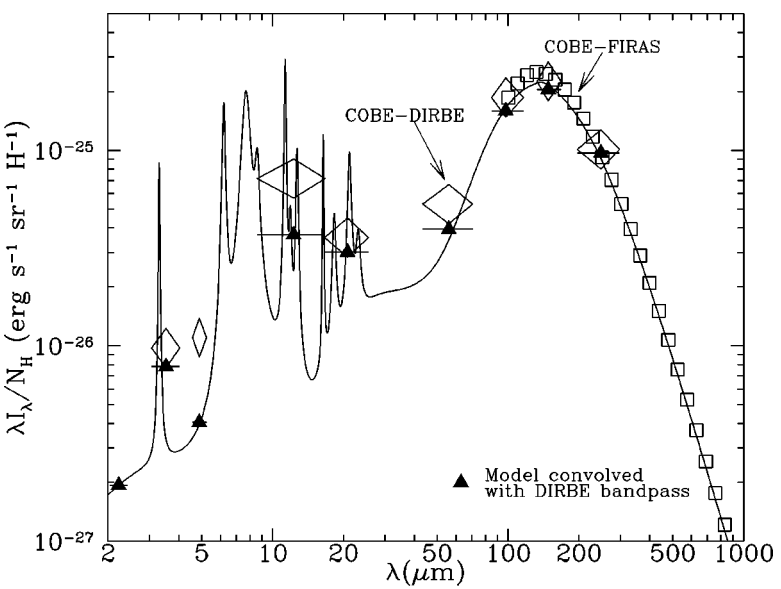

Figure 15 Solid line: infrared emission calculated for WD01 $R_V = 3.1$ Milky Way dust model (but with abundances reduced by factor 0.93) for grains heated by diffuse starlight (Li & Draine 2001b). Squares: COBE-FIRAS (Finkbeiner et al. 1999) Diamonds: COBE-DIRBE (Arendt et al. 1998).

The far-infrared emission is a good tracer of interstellar dust. The IRAS and DIRBE all-sky maps can be used to infer the dust column density (Schlegel et al. 1998).

10. MICROWAVE EMISSION

10.1. Spinning Grains

Theoretical models to account for the observed infrared emission require large numbers of extremely small dust grains that, following absorption of starlight photons, radiate in their optically active vibrational modes. In addition to vibrating, these grains will rotate, with rotation rates reaching tens of GHz. If they have electric dipole moments, there will be rotational emission from these grains at microwave frequencies. Various workers have considered microwave emission from spinning grains (Erickson 1957, Hoyle & Wickramasinghe 1970, Ferrara & Dettmar 1994). The rotational emission from this grain population has been estimated by Draine & Lazarian (1998a,b), who showed that it could account for dust-correlated microwave emission that was discovered by Kogut et al. (1996a,b) in studies of the angular structure of the cosmic microwave background.

The theoretical estimate for the rotational emission, plus the low-frequency tail of the vibrational emission, is shown in Figure 16. Figure 16 also shows results from a number of observational studies—some over large areas of the sky, others over smaller regions. Finkbeiner et al. (2002) detect dust-correlated microwave emission in pointed observations of a dark cloud (L1622) and toward LPH 201.663+1.643, a diffuse HII region behind heavy obscuration. Most recently, Finkbeiner et al. (2003a) use 8 GHz and 14 GHz surveys to map the anomalous microwave emission from the Galactic plane.

With the exception of the observations toward LPH 201.663+1.643, the observed microwave emission appears to be generally consistent with the theoretical prediction for emission from spinning dust grains.

The observed microwave emission from LPH 201.663+1.643 is, however, an order of magnitude stronger than would be expected from the observed column of dust. Although the rotational emission from spinning dust grains does depend on environment (Draine & Lazarian 1998b), it does not appear possible to explain the strong emission observed in this direction using reasonable variations in environmental conditions.

10.2. Magnetic Grains?

Although rotational emission from spinning grains is a natural prediction for a dust model with large numbers of small grains, other emission mechanisms are also possible, including thermal magnetic dipole radiation from magnetic grains (Draine & Lazarian 1999). We know that Fe contributes a significant fraction of the interstellar dust mass; if some of this Fe is in ferrimagnetic or ferromagnetic

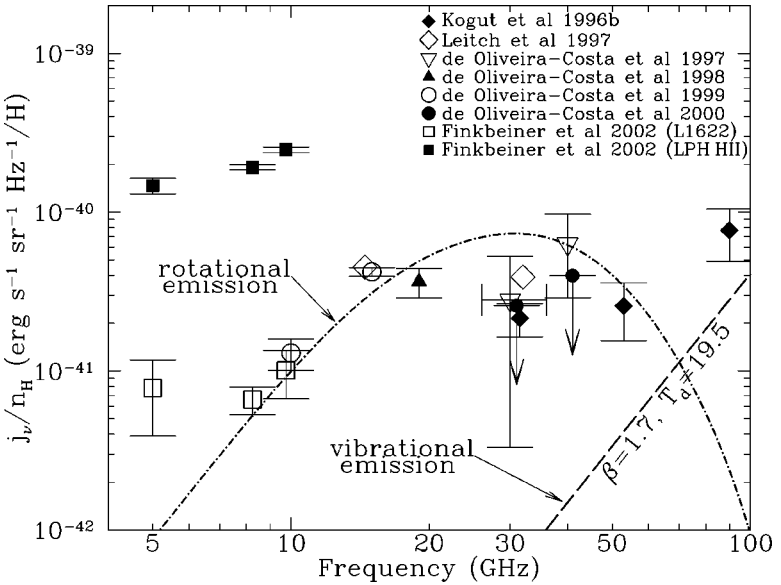

Figure 16 Dust-correlated microwave emission, expressed as microwave surface brightness per unit column density of hydrogen. Curves: theoretical estimate of Draine & Lazarian (1998a,b). Symbols: observational determinations of "anomalous microwave emission."

compounds, grains containing these compounds would emit magnetic dipole radiation. The idea is that the magnetization of the magnetic domains in the grain would fluctuate around the minimum-energy state; these fluctuations would be at GHz frequencies, and the fluctuating magnetization would generate electromagnetic radiation. If an appreciable fraction of the Fe in interstellar grains were in magnetite Fe_3O_4, it is estimated that the resulting thermal magnetic dipole emission would be comparable to the observed microwave emission. The power radiated per grain is simply proportional to the mass of magnetic material in that grain and proportional to the grain temperature. Because it is presumed that most of the magnetic material would be in large grains, it would be expected that the large grains would account for the bulk of the magnetic dipole emission.

It is therefore possible that the observed microwave emission may contain appreciable contributions from both (ultrasmall) spinning grains and (large) magnetic grains.

11. ABUNDANCE ISSUES

Dust population models that are constructed to reproduce the observed wavelength-dependent extinction are found to imply substantial abundances of elements in grain material—approaching or exceeding the abundances believed to be

appropriate to interstellar matter. Kim & Martin (1996) referred to the "C/H crisis", and Mathis (1996) has argued that the problem may be even more severe for Mg, Si, and Fe required for silicate grains.

Whether there is a problem or not depends on the adopted values for total interstellar abundances. Mathis (1996) took the position that interstellar abundances should be taken to be ∼70% of solar. However, recent changes in inferred solar abundances for C and O, and comparison of photospheric abundances in F and G stars with those in B stars, led Sofia & Meyer (2001) to reject the hypothesis that interstellar abundances are appreciably subsolar. Sofia & Meyer estimate the dust-phase abundances on the sightline to ζ Oph if interstellar abundances are taken to be the same as photospheric abundances in F and G stars. From these abundances we can construct carbon grains with volume $= 2.05 \times 10^{-27}$ cm^3/H (for an assumed $\rho = 2.2$ g cm^{-3}) and silicate/SiO_2 grains with volume 2.90×10^{-27} cm^3/H (for an assumed $\rho = 3.5$ g cm^{-3}).

The provisional grain model of §7—the Weingartner & Draine (2001a) grain model with abundances reduced by a factor 0.93—requires a carbonaceous grain volume $V_{\rm carb} = 2.10 \times 10^{-27}$ cm^3/H and a silicate grain volume $V_{\rm sil} = 3.68 \times 10^{-27}$ cm^3/H; thus we see that the carbon abundance is in line with observations, but the provisional grain model requires ∼26% more Mg, Si, and Fe than appears to be available. Is this 26% discrepancy a serious problem? Consider the following information:

1. Six of the 14 sightlines in Figure 2 have $A_I/N_{\rm H}$ differing by more than 30% from the nominal value. This may represent measurement errors but suggests real variations in $A_I/N_{\rm H}$. Because it is not clear how the sample of sightlines is constructed, it is not apparent that the average value of $A_I/N_{\rm H}$ for the sample is the same as the overall dust-to-gas ratio for the ISM.
2. The dust model assumes the grains to be spheres. Real grains are nonspherical. This will tend to provide somewhat more extinction per unit mass of grain material; this could increase the visual extinction per unit grain mass by ∼10%–20%.
3. The dust model assumes the grains to be compact, but real grains may contain voids. This could conceivably increase the visual extinction per unit grain mass by ∼10%.
4. The dust model uses bulk optical constants and Mie theory. The outer few monolayers of grain material, however, will have electronic structure (and therefore optical properties) differing from bulk material, so that the model calculations should not be considered to be precise even if the grains were actually spheres and we had the correct bulk optical constants.

At the present stage of observational and theoretical knowledge, we do not consider the apparent abundance crisis to be sufficient grounds to reject our provisional grain model, but new data could change this conclusion.

12. GRAIN ALIGNMENT

The polarization of starlight (see Section 6) was discovered more than 50 years ago (Hall 1949, Hiltner 1949) and was immediately recognized as being due to aligned dust grains. The mechanism responsible for the alignment has been sought by theorists for the past half-century. Two separate alignments are involved: (*A*) Alignment of the grain's principal axis of largest moment of inertia with the grain's angular momentum **J** and (*B*) alignment of **J** with the galactic magnetic field.

The alignment processes turn out to involve quite subtle physics [for an introduction, see Draine (2003a)]. The paramagnetic dissipation process proposed by Davis & Greenstein (1951) would be able to gradually align grains, but recent work shows that radiative torques due to starlight can be much stronger than the Davis-Greenstein torque; the starlight torques can affect both the rate of grain rotation—driving grains to suprathermal rotation rates—as well as the direction of the grain angular momentum (Draine & Weingartner 1996, 1997). The electronic and nuclear paramagnetism of the grain couple the rotational degrees of freedom to the vibrational degrees of freedom, with important consequences for the rotational dynamics of a tumbling grain (Lazarian & Draine 1999a,b).

H_2 formation on grain surfaces is thought to take place at a limited number of reaction sites, and the recoil from nascent H_2 provides a systematic torque on the grain that is fixed in body coordinates (Purcell 1979) and that can drive a grain to suprathermal rotation rates. When the grain rotational kinetic energy is not too large compared to kT_d, where T_d is the grain temperature, the process of "thermal flipping" (Lazarian & Draine 1999a) can cause the H_2 formation torque to time-average to zero, so that suprathermal rotation does not take place—a process termed "thermal trapping." Radiative torques due to starlight, however, are not fixed in grain body coordinates and therefore do not time-average to zero even when thermal flipping is rapid, so that grains subject to starlight torques are immune to thermal trapping and are expected to rotate suprathermally most of the time. Starlight torques are important only for grains with radii $a \gtrsim 0.1\ \mu$m. This may explain the fact that grains with radii $a \gtrsim 0.2\ \mu$m appear to be much more strongly aligned than grains with radii $a \lesssim 0.05\ \mu$m (Kim & Martin 1995).

The theory of grain alignment is complicated by the need to describe the dynamics of tumbling grains during intervals when the grain rotational kinetic energy is of order $kT_{\rm gas}$, including the effects of thermal flipping (Weingartner & Draine 2003). Progress is being made, and quantitative calculations of grain alignment for model grains should be possible within the next year or two—this should allow us to predict the wavelength-dependent polarization for a grain model once a geometric asymmetry is assumed for the grains. At that time we will learn whether our current picture of grain dynamics is consistent with observations.

The very smallest grains spin with GHz rotation rates and emit electric dipole radiation in the microwave (see Section 10). If these grains are aligned with the magnetic field, the rotational emission will be polarized. It appears, however, that

these grains will be only minimally aligned, with degrees of alignment of only a few percent (Lazarian & Draine 2000). The Davis-Greenstein paramagnetic dissipation mechanism is suppressed in these grains by the unavailability of vibrational modes with energies $\hbar\omega_{\rm rot}$.

13. EVOLUTION OF THE GRAIN POPULATION

The interstellar grain population in a galaxy reflects the interplay of many processes.

Are interstellar grains "stardust"? There is ample evidence that grains form in some stellar outflows—we see infrared emission from dust in outflows from red giants and carbon stars, and in planetary nebulae. In all of these cases it is believed that the bulk of the dust condensed out of initially dust-free gas from the stellar envelope. The 10 μm silicate feature is seen in outflows from oxygen-rich stars, consistent with the expectation that silicates should be a major condensate in cooling gas with O/C $>$ 1. The 10 μm feature is not seen in outflows from stars with C/O $>$ 1, where instead one sometimes sees a feature at 11.3 μm that is attributed to SiC (Treffers & Cohen 1974, Blanco et al. 1998), consistent with the expected condensates from cooling gas with O/C $<$ 1. Because isotopic anomalies are used to find them, presolar grains in meteorites generally appear to be "stardust"—a given grain was formed in the outflow/ejecta from a single star with a particular isotopic composition.

There is no doubt that dust is formed in many stellar outflows. However, this does not imply that the bulk of the dust in the ISM was produced in this way. The problem is that interstellar grains are subject to sputtering (Draine & Salpeter 1979a), and grain-grain collisions in interstellar shock waves and theoretical studies of grain destruction in the Milky Way find a mean "residence time" of an atom in a grain of order $\tau_{\rm dest} \approx 3\times10^8$ yr (Draine & Salpeter 1979b, Jones et al. 1994).

Now suppose that all Si atoms enter the ISM as constituents of dust grains. The total mass of the ISM is $M_{\rm ISM} \approx 5\times10^9\ M_\odot$, and star formation takes place at a rate $\dot{M}_\star \lesssim 5\ M_\odot\ {\rm yr}^{-1}$. Thus, the mean residence time of a metal atom in the ISM is $\tau_{\rm ISM} = M_{\rm ISM}/\dot{M}_\star \approx 10^9$ yr. Only a fraction $\tau_{\rm dest}/(\tau_{\rm dest}+\tau_{\rm ISM}) \approx 0.2$ of the Si atoms in the ISM would be found in the original stardust particle in which they left a star.

However, when we observe gas-phase abundances in the ISM, we typically find $\gtrsim$90% of the Si atoms missing from the gas phase. Unless we have grossly underestimated the grain destruction time $\tau_{\rm dest}$, it must follow that most of the Si atoms in interstellar grains joined the grain in the ISM. Therefore, most interstellar dust is not stardust—the composition of interstellar grains is determined by physical processes in the ISM. The importance of interstellar processing is also evident from the large variations seen in the extinction curve from one sightline to another—these variations must be the result of interstellar effects because any given sightline would be expected to average over the stardust produced by many individual stars. The interstellar processes that alter grains include the following:

- grain erosion by sputtering
- grain shattering in low-velocity grain-grain collisions
- grain vaporization in high-velocity grain-grain collisions
- grain coagulation
- accretion of impinging atoms and molecules on grain surfaces
- chemical reaction of impinging atoms and radicals with grain surfaces
- photolysis of grain material by UV starlight
- alteration of grain material by cosmic ray/X-ray irradiation
- photodesorption of atoms and molecules from grain surfaces

In addition, the local grain mixture can be modified by size- and composition-dependent drift of dust through the gas, driven by anisotropic starlight: Relative drift speeds $\gtrsim 0.1$ km s^{-1} can displace large grains from small grains by $\gtrsim 1$ pc in 10^7 yr (Weingartner & Draine 2001b).

Understanding the balance among these different processes requires not only an understanding of the microscopic physics but also a quantitative model for the transport of grains from one phase of the ISM to another. Because grain destruction appears to be dominated by processes associated with interstellar shock waves, the propagation of these shock waves through the inhomogeneous ISM must be modeled.

The required modeling is complex, and we are not yet at a stage where a priori modeling of the evolution of the interstellar grain population can be considered reliable. However, the observed depletions can be used to constrain models of the dynamic ISM: In order for grains to be able to "scavenge" elements like Si from the gas, there must be rapid "cycling" of matter between the diffuse low-density phases (where most grain destruction takes place) and denser regions (where densities are high enough for grain growth to be effective), with cycling times as short as $\sim 10^7$ yr (Draine 1990).

14. FUTURE DIRECTIONS

Our present understanding of interstellar grains is built upon an observational base. Additional observational constraints—which could conceivably require revisions to our models—will be provided by a number of new facilities, including the following:

- SIRTF (Space InfraRed Telescope Facility) will provide low- and medium-resolution 5–40 μm spectra of reflection nebulae, 55–96 μm spectral energy distributions, and imaging in seven photometric bands from 3.5 to 160 μm. We can anticipate detection of new emission features in the 15–40 μm region (where ISO had limited sensitivity) and studies of variations of dust emission features and spectra with environment.

- Astro-F (Pearson et al. 2002, and references therein), scheduled for launch in 2004, will obtain all-sky maps in four bands between 50 and 200 μm, with improved spatial resolution and much better sensitivity than IRAS. This will greatly improve our knowledge of the distribution of diffuse dust, the degree to which dust is correlated with H I 21 cm emission, and spatial variations in the far-infrared band ratios. Astro-F may be able to provide all-sky imaging in 6–11 μm that would provide a map of PAH emission. Correlation of the PAH emission with microwave emission would test the hypothesis that the microwave emission comes from spinning grains.
- WMAP (Wilkinson Microwave Anisotropy Probe) is producing maps of the microwave sky in five bands between 22 and 90 GHz, with FWHM of 0.53° at 40 GHz. These maps will help to characterize the spectrum of the microwave emission from dust, as well as variations in dust emission (intensity and spectrum) from one region to another (Bennett et al. 2003). It will be of great interest to cross-correlate the all-sky microwave maps with infrared and far-infrared maps from IRAS, COBE, and, when available, Astro-F.
- Planck/Surveyor, scheduled for launch in 2007, will provide all-sky submm maps that will determine the diffuse dust emission spectrum from 30–857 GHz (1 cm–350 μm).
- Herschel, scheduled for launch together with Planck, will be capable of sensitive broadband diffraction-limited imaging at 60–700 μm, extending beyond the 160 μm cutoff of SIRTF. The longer wavelength coverage will provide improved determinations of the emission from cool dust and will allow a census of dust masses in nearby galaxies.
- The Stardust spacecraft is expected to return to Earth in 2006. Its aerogel panels will have interstellar grain material at impact sites and (we hope) intact cometary dust particles.
- SOFIA (Stratospheric Observatory for Infrared Astronomy) will provide higher angular resolution dust emission imaging between 5 and 240 μm.
- Ground-based millimeter and submillimeter telescopes and arrays (e.g., BIMA, JCMT, CSO, ALMA) can map thermal dust emission from dense regions, including polarimetric mapping.

Many problems await solution, some of which are highlighted here:

- The carrier of the 2175 Å feature remains unidentified. The PAHs required by the observed IR emission features are expected to produce strong absorption in this region, but this remains conjecture. We require lab measurements of UV absorption by PAH molecules, radicals, and ions containing $20–10^3$ C atoms for comparison with the observed 2175 Å profile.
- The nature of the ERE carrier remains an open question. The high intensities reported for diffuse clouds imply that the ERE carrier must be a major grain

constituent (see Section 3.8). Further observations of the ERE are needed, particularly to confirm the intensity of ERE from diffuse clouds. Further spectroscopy of ERE emission from bright regions, and laboratory studies of candidate ERE carriers, may lead to identification of the ERE carrier.

- We should be able to identify at least some of the DIBs. Gas-phase spectroscopy of candidate molecules, radicals, and ions is needed. When the right candidates are studied, positive spectroscopic identification of DIBs will follow.
- PAH molecules, radicals, and ions appear to be a major part of the grain population in the Milky Way, but the origin of these PAHs is unknown. Further observational study of spatial variations in PAH abundance (and perhaps spectral properties) may provide valuable clues.
- We would like to understand the balance of processes (growth, coagulation, erosion, shattering) accounting for the size distribution of interstellar dust. Observational determinations of regional variations in the size distribution will frame the theoretical attack on this problem.
- Are there really separate populations of carbonaceous grains and silicate grains? If so, how does grain growth in the ISM maintain these separate populations?
- Is the anomalous microwave emission due primarily to spinning dust grains? Is there a significant contribution from magnetic dust materials (see Section 10)?
- Can we diagnose the composition of interstellar dust using X-ray absorption measurements (see Section 3.7)?
- The problem of interstellar grain alignment (see Section 12) seems ripe for solution. Radiative torques due to starlight appear to be an important part of the alignment process. A solution to this problem may be in sight.

I thank D. Finkbeiner, D. Gutkowicz-Krusin, A. Li, and J. Weingartner for helpful comments and RH Lupton for availability of the SM software package. This research was supported in part by NSF grant AST-9988126.

The *Annual Review of Astronomy and Astrophysics* is online at http://astro.annualreviews.org

LITERATURE CITED

Adamson AJ, Whittet DCB. 1995. *Ap. J.* 448:L49–52

Adamson AJ, Whittet DCB, Duley WW. 1990. *MNRAS* 243:400–4

Aitken DK, Smith CH, Roche PF. 1989. *MNRAS* 236:919–27

Allamandola LJ, Tielens AGGM, Barker JR. 1989. *Ap. J. Suppl.* 71:733–75

Anderson CM, Weitenbeck AJ, Code AD, Nordsieck KH, Meade MR, et al. 1996. *Astron. J.* 112:2726–43

Arendt RG, Odegard N, Weiland JL, Sodroski

TJ, Hauser MG, et al. 1998. *Ap. J.* 508:74–105
Artymowicz P. 2000. *Space Sci. Rev.* 92:69–86
Bennett C, Hill RS, Hinshaw G, Nolta MR, Odegard N, et al. 2003. *Ap. J.* Submitted (astro-ph/0302208)
Berlind AA, Quillen AC, Pogge RW, Sellgren K. 1997. *Astron. J.* 114:107–14
Bernstein RA, Freedman WL, Madore BF. 2002. *Ap. J.* 571:107–28
Bertoldi F, Timmermann R, Rosenthal D, Drapatz S, Wright CM. 1999. *Astron. Astrophys.* 346:267–77
Bessell MS, Brett JM. 1988. *Publ. Astron. Soc. Pac.* 100:1134–51
Bianchi L, Clayton GC, Bohlin RC, Hutchings JB, Massey P. 1996. *Ap. J.* 471:203–10
Blanco A, Borghesi A, Fonti S, Orofino V. 1998. *Astron. Astrophys.* 330:505–14
Bohlin RC, Savage BD, Drake JF. 1978. *Ap. J.* 224:132–42
Boulanger F, Perault M. 1988. *Ap. J.* 330:964–85
Bouwman J, Meeus G, de Koter A, Hony S, Dominik C, Waters LBFM. 2001. *Astron. Astrophys.* 375:950–62
Bowey JE, Adamson AJ. 2002. *MNRAS* 334:94–106
Bowey JE, Adamson AJ, Whittet DCB. 1998. *MNRAS* 298:131–38
Bradley JP. 1994. *Science* 265:925–29
Bradley JP, Keller LP, Snow TP, Hanner MS, Flynn GJ, et al. 1999. *Science* 285:1716–18
Brownlee DE. 1985. *Annu. Rev. Earth Planet. Sci.* 13:147–73
Brownlee DE, Tsou P, Clark B, Hanner MS, Hörz F, et al. 2000. *Meteor. Planet. Sci.* 35(Suppl.):A35
Burgh EB, McCandliss SR, Feldman PD. 2002. *Ap. J.* 575:240–49
Calzetti D. 2001. *Publ. Astron. Soc. Pac.* 113:1449–85
Calzetti D, Bohlin RC, Gordon KD, Witt AN, Bianchi L. 1995. *Ap. J. Lett.* 446:L97–100
Cardelli JA, Clayton GC, Mathis JS. 1989. *Ap. J.* 345:245–56
Catura RC. 1983. *Ap. J.* 275:645–651
Cesarsky D, Lequeux J, Abergel A, Perault M, Palazzi E, et al. 1996. *Astron. Astrophys.* 315:L305–8
Chiar JE, Tielens AGGM, Whittet DCB, Schutte WA, Boogert ACA, et al. 2000. *Ap. J.* 537:749–62
Chihara H, Koike C, Tsuchiyama A, Tachibana S, Sakamoto D. 2002. *Astron. Astrophys.* 391:267–73
Chrysostomou A, Aitken DK, Jenness T, Davis CJ, Hough JH, et al. 2002. *Astron. Astrophys.* 385:1014–21
Chrysostomou A, Hough JH, Whittet DCB, Aitken DK, Roche PF, Lazarian A. 1996. *Ap. J. Lett.* 465:L61–64
Clark GW, Woo JW, Nagase F. 1994. *Ap. J.* 422:336–50
Clayton GC, Mathis JS. 1988. *Ap. J.* 327:911–19
Clayton GC, Wolff MJ, Allen RG, Lupie OL. 1996. *Ap. J.* 445:947–57
Darbon S, Perrin JM, Sivan JP. 1999. *Astron. Astrophys.* 348:990–92
Darbon S, Zavagno A, Perrin JM, Savine C, Ducci V, Sivan JP. 2000. *Astron. Astrophys.* 364:723–31
Davis L, Greenstein JL. 1951. *Ap. J.* 114:206–40
Day KL. 1979. *Ap. J.* 234:158–61
Demyk K, Jones AP, Dartois E, Cox P, d'Hendecourt L. 1999. *Astron. Astrophys.* 349:267–75
de Oliveira-Costa A, Kogut A, Devlin MJ, Netterfield CB, Page LA, Wollack EJ. 1997. *Ap. J. Lett.* 482:L17–20
de Oliveira-Costa A, Tegmark M, Devlin MJ, Haffner LM, Herbig TM, et al. 2000. *Ap. J. Lett.* 542:L5–8
de Oliveira-Costa A, Tegmark M, Gutiérrez CM, Jones AW, Davies RD, et al. 1999. *Ap. J. Lett.* 527:L9–12
de Oliveira-Costa A, Tegmark M, Page LA, Boughn SP. 1998. *Ap. J. Lett.* 509:L9–12
Désert FX, Jenniskens P, Dennefeld M. 1995. *Astron. Astrophys.* 303:223–32
d'Hendecourt LB, Léger A, Olofson G, Schmidt W. 1986. *Astron. Astrophys.* 170: 91–96

Dorschner J, Henning T. 1995. *Astron. Astrophys. Rev.* 6:271–333
Dotson JL, Davidson J, Dowell CD, Schleuning DA, Hildebrand RH. 2000. *Ap. J. Suppl.* 128:335–70
Draine BT. 1989a. In *Proc. IAU Symp. 135, Interstellar Dust*, ed. LJ Allamandola, AGGM Tielens, pp. 313–27. Dordrecht: Kluwer
Draine BT. 1989b. In *Infrared Spectroscopy in Astronomy*, ed. BH Kaldeich, pp. 93–98. Noordwijk: ESA
Draine BT. 1990. In *The Evolution of the Interstellar Medium*, ed. L Blitz, pp. 193–205. San Francisco: Astron. Soc. Pac.
Draine BT. 1995. In *Physics of the Interstellar Medium and Intergalactic Medium*, ed. A Ferrara, C Heiles, CF McKee, PR Shapiro, pp. 133–47. San Francisco: Astron. Soc. Pac.
Draine BT. 2003a. In *The Cold Universe*, ed. D Pfenniger. Berlin: Springer-Verlag. In press (astro-ph/0304488)
Draine BT. 2003b. *Ap. J.* submitted (astro-ph/0304060)
Draine BT, Lazarian A. 1998a. *Ap. J. Lett.* 459:L19–22
Draine BT, Lazarian A. 1998b. *Ap. J.* 508:157–79
Draine BT, Lazarian A. 1999. *Ap. J.* 512:740–54
Draine BT, Lee HM. 1984. *Ap. J.* 285:89–108
Draine BT, Li A. 2001. *Ap. J.* 551:807–24
Draine BT, Malhotra S. 1993. *Ap. J.* 414:632–45
Draine BT, Salpeter EE. 1979a. *Ap. J.* 231:77–94
Draine BT, Salpeter EE. 1979b. *Ap. J.* 231:438–55
Draine BT, Tan JC. 2003. *Ap. J.* Submitted (astro-ph/0208302)
Draine BT, Weingartner JC. 1996. *Ap. J.* 470:551–65
Draine BT, Weingartner JC. 1997. *Ap. J.* 480:633–46
Dufour RJ. 1984. In *IAU Symp. 108, Structure and Evolution of the Magellanic Clouds*, ed. S van den Bergh, KS de Boer, pp. 353–60. Dordrecht: Reidel
Duley WW. 1985. *MNRAS* 215:259–63
Duley WW, Scott AD, Seahra S, Dadswell G. 1998. *Ap. J. Lett.* 503:L183–85
Ehrenfreund P, Cami J, Jiménez-Vicente J, Foing BH, Kaper L, et al. 2002. *Ap. J. Lett.* 576:L117–20
Erickson WC. 1957. *Ap. J.* 126:489–92
Falco EE, Impey CD, Kochanek CS, Lehár J, McLeod BA, et al. 1999. *Ap. J.* 523:617–32
Ferrara A, Dettmar R.-J. 1994. *Ap. J.* 427:155–59
Finkbeiner DP, Davis M, Schlegel DJ. 1999. *Ap. J.* 524:867–86
Finkbeiner DP, Langston G, Minter T. 2003a. *Bull. AAS* 34 #140.05
Finkbeiner DP, Schlegel DJ, et al. 2003b. In preparation
Finkbeiner DP, Schlegel DJ, Frank C, Heiles C. 2002. *Ap. J.* 566:898–904
Fitzpatrick EL. 1985. *Ap. J.* 299:219–35
Fitzpatrick EL. 1986. *Astron. J.* 92:1068–73
Fitzpatrick EL. 1997. *Ap. J. Lett.* 482:L199–202
Fitzpatrick EL. 1999. *Publ. Astron. Soc. Pac.* 111:63–75
Fitzpatrick EL, Massa D. 1986. *Ap. J.* 307:286–94
Forrey RC, Woo JW, Cho K. 1998. *Ap. J.* 505:236–43
Frisch PC, Dorschner JM, Geiss J, Greenberg JM, Grün E, et al. 1999. *Ap. J.* 525:492–516
Fukugita M, Ichikawa T, Gunn JE, Doi M, Shimasaku K, Schneider DP. 1996. *Astron. J.* 111:1748–56
Furton DG, Witt AN. 1990. *Ap. J. Lett.* 364:L45–48
Furton DG, Witt AN. 1993. *Ap. J. Lett.* 415:L51–54
Gerakines PA, Whittet DCB, Ehrenfreund P, Boogert ACA, Tielens AGGM, et al. 1999. *Ap. J.* 522:357–77, 526:1062
Gibb EL, Whittet DCB, Schutte WA, Boogert ACA, Chiar JE, et al. 2000. *Ap. J.* 536:347–56
Gibson SJ, Nordsieck KH. 2003. *Ap. J.* 589: 362–77
Gillett FC, Forrest WJ, Merrill KM, Soifer BT, Capps RW. 1975. *Ap. J.* 200:609–20

Goodman AA, Jones TJ, Lada EA, Myers PC. 1995. *Ap. J.* 448:748–65
Gordon KD, Witt AN, Carruthers GR, Christensen SA, Dohne BC. 1994. *Ap. J.* 432:641–7
Gordon KD, Witt AN, Friedmann BC. 1998. *Ap. J.* 498:522–40
Gordon KD, Witt AN, Rudy RJ, Puetter RC, Lynch DK, et al. 2000. *Ap. J.* 544:859–66
Greenberg JM, Li A, Mendoza-Gómez CX, Schutte WA, Gerakines PA, de Groot M. 1995. *Ap. J. Lett.* 455:L177–80
Grevesse N, Sauval AJ. 1998. *Space Sci. Rev.* 85:161–74
Guhathakurta P, Draine BT. 1989. *Ap. J.* 345:230–44
Gürtler J, Klaas U, Henning Th, Ábrahám P, Lemke D, et al. 2002. *Astron. Astrophys.* 390:1075–87
Haikala LK, Mattila K, Bowyer S, Sasseen TP, Lampton M, Knude J. 1995. *Ap. J. Lett.* 443:L33–36
Hall JS. 1949. *Science* 109:166
Hanner MS. 1999. *Space Sci. Rev.* 90:99–108
Hayakawa S. 1970. *Prog. Theor. Phys.* 43: 1224–30
Heger ML. 1922. *Lick Obs. Bull.* 10:146–47
Hildebrand RH, Dotson JL, Dowell CD, Schleuning DA, Vaillancourt JE. 1999. *Ap. J.* 516:834–42
Hiltner WA. 1949. *Science* 109:165
Hoppe PM, Zinner E. 2000. *J. Geophys. Res.* 105:10371–85
Hough JH, Chrysostomou A, Messinger DW, Whittet DCB, Aitken DK, Roche PF. 1996. *Ap. J.* 461:902–8
Howk JC, Savage BD, Fabian D. 1999. *Ap. J.* 525:253–93
Hoyle F, Wickramasinghe NC. 1970. *Nature* 227:473–74
Hurwitz M, Bowyer S, Martin C. 1991. *Ap. J.* 372:167–84
Jäger C, Molster FJ, Dorschner J, Henning Th, Mutschke H, Waters LBFM. 1998. *Astron. Astrophys.* 339:904–16
Jäger C, Mutschke H, Begemann B, Dorschner J, Henning Th. 1994. *Astron. Astrophys.* 292:641–55
Jenniskens P, Desert FX. 1994. *Astron. Ap. Suppl.* 106:39–78
Johnson HL. 1965. *Ap. J.* 141:923–42
Jones AP, Tielens AGGM, Hollenbach DJ, McKee CF. 1994. *Ap. J.* 433:797–810
Keane JV, Tielens AGGM, Boogert ACA, Schutte WA, Whittet DCB. 2001. *Astron. Astrophys.* 376:254–70
Keel WC, White RE. 2001a. *Astron. J.* 121:1442–55
Keel WC, White RE. 2001b. *Astron. J.* 122:1369–82
Kemper F, Jäger C, Waters LBFM, Henning Th, Molster FJ, et al. 2002. *Nature* 415:295–97
Kerr TH, Hibbins RE, Fossey SJ, Miles JR, Sarre PJ. 1998. *Ap. J.* 495:941–45
Kerr TH, Hibbins RE, Miles JR, Fossey SJ, Sommerville WB, Sarre PJ. 1996. *MNRAS* 283:1104–9
Kim S-H, Martin PG. 1995. *Ap. J.* 444:293–305
Kim S-H, Martin PG. 1996. *Ap. J.* 462:296–308
Kogut A, Banday AJ, Bennett CL, Górski KM, Hinshaw G, Reach WT. 1996a. *Ap. J.* 460:1–9
Kogut A, Banday AJ, Bennett CL, Górski KM, Hinshaw G, et al. 1996b. *Ap. J. Lett.* 464:L5–9
Koike C, Tsuchiyama A. 1992. *MNRAS* 255: 248–54
Koike C, Tsuchiyama A, Suto H, et al. 1999. In *Proc. 32nd ISAS Lunar Planetary Symp.*, 32:175
Koorneef J. 1982. *Astron. Astrophys.* 107:247–51
Kraetschmer W, Huffman DR. 1979. *Ap. Space Sci.* 61:195–203
Krügel E. 2002. *The Physics of Interstellar Dust*. Bristol: Institute of Physics
Kurt CM, Dufour RJ. 1998. *Rev. Mex. Astron. Astrofis.* 7:202–6
Lacy JH, Faraji H, Sandford SA, Allamandola LJ. 1998. *Ap. J. Lett.* 501:L105–9
Lai SP, Crutcher RM, Girart JM, Rao R. 2001. *Ap. J.* 561:864–70
Laor A, Draine BT. 1993. *Ap. J.* 402:441–68
Laureijs RJ, Mattila K, Schnur G. 1987. *Astron. Astrophys.* 184:269–78

Lazarian A, Draine BT. 1999a. *Ap. J. Lett.* 516:L37–40
Lazarian A, Draine BT. 1999b. *Ap. J. Lett.* 520:L67–70
Lazarian A, Draine BT. 2000. *Ap. J. Lett.* 536:L15–18
Ledoux G, Ehbrecht M, Guillois O, Huisken F, Kohn B, et al. 1998. *Astron. Astrophys.* 333:L39–42
Leger A, Puget JL. 1984. *Astron. Astrophys.* 137:L5–8
Lehtinen K, Mattila K. 1996. *Astron. Astrophys.* 309:570–80
Leitch EM, Readhead ACS, Pearson TJ, Myers ST. 1997. *Ap. J. Lett.* 486:L23–26
Li A, Draine BT. 2001a. *Ap. J. Lett.* 550:L213–17
Li A, Draine BT. 2001b. *Ap. J.* 554:778–802
Li A, Draine BT. 2002a. *Ap. J.* 564:803–12
Li A, Draine BT. 2002b. *Ap. J.* 572:232–37
Li A, Draine BT. 2002c. *Ap. J.* 576:762–77
Li A, Greenberg JM. 1997. *Astron. Astrophys.* 323:566–84
Li A, Greenberg JM. 2002. *Ap. J.* 577:789–94
Lillie CF, Witt AN. 1976 *Ap. J.* 208:64–76
Lupton RH, Ivezic Z, et al. 2003. In preparation
Lutz D, Feuchtgruber H, Genzel R, Kunze D, Rigopoulou D, et al. 1996. *Astron. Astrophys.* 315:L269–72
Malhotra S. 1997. *Ap. J. Lett.* 488:L101–4
Martin N, Maurice E, Lequeux J, 1989. *Astron. Astrophys.* 215:219–42
Martin PG. 1970. *MNRAS* 149:221–35
Martin PG. 1975. *Ap. J.* 292:393–99
Martin PG, Angel JRP. 1974. *Ap. J.* 188:517–22
Martin PG, Whittet DCB. 1990. *Ap. J.* 357:113–24
Mathis JS. 1990. *Annu. Rev. Astron. Astrophys.* 28:37–70
Mathis JS. 1993. *Rep. Prog. Phys.* 56:605–52
Mathis JS. 1996. *Ap. J.* 472:643–55
Mathis JS. 1998. *Ap. J.* 497:824–32
Mathis JS. 2000. *J. Geophys. Res.* 105:10269–77
Mathis JS, Cohen D, Finley JP, Krautter J. 1995. *Ap. J.* 449:320–29
Mathis JS, Lee C-W. 1991. *Ap. J.* 376:490–99
Mathis JS, Rumpl W, Nordsieck KH. 1977. *Ap. J.* 217:425–33
Mathis JS, Whiffen G. 1989. *Ap. J.* 341:808–22
Mattila K. 1970. *Astron. Astrophys.* 9:53–63
Mauche CW, Gorenstein P. 1986. *Ap. J.* 302: 371–87
McCarthy JF, Forrest WJ, Briotta DA, Houck JR. 1980. *Ap. J.* 242:965–975
McKee CF, Petrosian V. 1974. *Ap. J.* 189:17–21
Mennella V, Colangeli L, Bussoletti E, Palumbo P, Rotundi A. 1998. *Ap. J. Lett.* 507:L177–80
Merrill PW. 1934. *Publ. Astron. Soc. Pac.* 46:206–7
Misselt KA, Clayton GC, Gordon KD. 1999. *Ap. J.* 515:128–39
Mitsuda K, Takeshima T, Kii T, Kawai N. 1990. *Ap. J.* 353:480–85
Molster FJ, Waters LBFM, Tielens AGGM. 2002a. *Astron. Astrophys.* 382:222–40
Molster FJ, Waters LBFM, Tielens AGGM, Koike C, Chihara H. 2002b. *Astron. Astrophys.* 382:241–55
Morgan DH, Nandy K, Thompson GI. 1976. *MNRAS* 177:531–44
Motta V, Mediavilla E, Muñoz JA, Falco E, Kochanek CS, et al. 2002. *Ap. J.* 574: 719–25
Murthy J, Henry RC. 1995. *Ap. J.* 448:848–57
Onaka T, Okada Y. 2003. *Ap. J.* 585:872–77
Onaka T, Yamamura I, Tanabe T, Roellig TL, Yuen L. 1996. *Publ. Astron. Soc. Jpn.* 48:L59–63
Overbeck JW. 1965. *Ap. J.* 141:864–66
Padoan P, Goodman A, Draine BT, Juvela M, Nordlund A, Rögnvaldsson ÖE. 2001. *Ap. J.* 559:1005–18
Paerels F, Brinkman AC, van der Meer RLJ, Kaastra JS, Kuulkers E, et al. 2001. *Ap. J.* 546:338–44
Papoular R, Conard J, Guillois O, Nenner I, Reynaud C, Rouzaud JN. 1996. *Astron. Astrophys.* 315:222–36
Pearson CP, Shibai H, Matsumoto T, Murakami H, Nakagawa T, et al. 2002. astro-ph/0210292v1 (*MNRAS*. Submitted)
Pendleton YJ, Allamandola LJ. 2002. *Ap. J. Suppl.* 138:75–98

Pierini D, Majeed A, Boroson TA, Witt AN. 2002. *Ap. J.* 569:184–203
Pitman KM, Clayton GC, Gordon KD. 2000. *Publ. Astron. Soc. Pac.* 112:537–41
Predehl P, Klose S. 1996. *Astron. Astrophys.* 306:283–93
Purcell EM. 1979. *Ap. J.* 231:404–16
Purcell EM, Shapiro PR. 1977. *Ap. J.* 214:92–105
Rachford BL, Snow TP, Tumlinson J, Shull JM, Blair WP, et al. 2002. *Ap. J.* 577:221–44
Rieke GH, Lebofsky MJ. 1985. *Ap. J.* 288:618–21
Roche PF, Aitken DK. 1984. *MNRAS* 208:481–92
Roche PF, Aitken DK. 1985. *MNRAS* 215:425–35
Rosenthal D, Bertoldi F, Drapatz S. 2000. *Astron. Astrophys.* 356:705–23
Rusli, Robertson J, Amaratunga GAJ. 1996. *J. Appl. Phys.* 80:2998–3003
Russell RW, Soifer BT, Forrest WJ. 1975. *Ap. J. Lett.* 198:L41–43
Sakata A, Wada S, Narisawa T, Asano Y, Iijima Y, et al. 1992. *Ap. J.* 393:L83–86
Sandford SA, Allamandola LJ, Tielens AGGM, Sellgren K, Tapia M, Pendleton Y. 1991. *Ap. J.* 371:607–20
Sandford SA, Pendleton YJ, Allamandola LJ. 1995. *Ap. J.* 440:697–705
Sasseen TP, Deharveng J-M. 1996. *Ap. J.* 469:691–97
Savage BD, Mathis JS. 1979. *Annu. Rev. Astron. Astrophys.* 17:73–111
Schiminovich D, Friedman PG, Martin C, Morrissey PF. 2001. *Ap. J. Lett.* 563:L161–64
Schlegel DJ, Finkbeiner DP, Blanton M, Gunn JE, Hogg DW. 2003. In preparation
Schlegel DJ, Finkbeiner DP, Davis M. 1998. *Ap. J.* 500:525–53
Schmidt GD, Cohen M, Margon B. 1980. *Ap. J. Lett.* 239:L133–38
Schulz NS, Cui W, Canizares CR, Marshall HL, Lee JC, et al. 2002. *Ap. J.* 556:1141–49
Schutte WA, van der Hucht KA, Whittet DCB, Boogert ACA, Tielens AGGM, et al. 1998. *Astron. Astrophys.* 337:261–74
Scott A, Duley WW. 1996. *Ap. J. Suppl.* 105:401–5
Seahra SS, Duley WW. 1999. *Ap. J.* 520:719–23
Serkowski K. 1973. In *IAU Symp. 52, Interstellar Dust and Related Topics*, ed. JM Greenberg, HC van de Hulst, pp. 145–52. Dordrecht: Reidel
Serkowski K, Mathewson DS, Ford VL. 1975. *Ap. J.* 196:261–90
Sivan JP, Perrin JM. 1993. *Ap. J.* 404:258–63
Smith CH, Wright CM, Aitken DK, Roche PF, Hough JH. 2000. *MNRAS* 312:327–61
Smith RK, Dwek E. 1998. *Ap. J.* 503:831–42
Smith RK, Edgar RJ, Shafer RA. 2002. *Ap. J.* 581:562–69
Smith TL, Gordon KD, Clayton GC. 2001. *Bull. AAS* 199 #11.06
Smith TL, Witt AN. 2002. *Ap. J.* 565:304–18
Sofia UJ, Meyer DM. 2001. *Ap. J. Lett.* 554:L221–24, 558:L147
Spitzer LS, Fitzpatrick EL. 1993. *Ap. J.* 409:299–318
Stecher TP. 1965. *Ap. J.* 142:1683–84
Stecher TP, Donn B. 1965. *Ap. J.* 142:1681–83
Steel TM, Duley WW. 1987. *Ap. J.* 315:337–39
Stephens JR, Blanco A, Bussoletti E, Colangeli L, Fonti S, et al. 1995. *Planet. Space Sci.* 43:1241–46
Suto H, Koike C, Sogawa H, Tsuchiyama A, Chihara H, Mizutani K. 2002. *Astron. Astrophys.* 389:568–71
Szomoru A, Guhathakurta P. 1998. *Ap. J. Lett.* 494:L93–97
Szomoru A, Guhathakurta P. 1999. *Astron. J.* 117:2226–43
Taban IM, Schutte WA, Pontoppidan KM, van Dishoeck EF. 2003. *Astron. Astrophys.* 399:169–75
Takei Y, Fujimoto R, Mitsuda, K, Onaka, T. 2002. *Ap. J.* 581:307–14
Tanaka M, Matsumoto T, Murakami H, Kawada M, Noda M, Matsuura S. 1996. *Publ. Astron. Soc. Jpn.* 48:L53–57
Tielens AGGM, Waters LBFM, Molster FJ, Justtanont K. 1998. *Ap. Space Sci.* 255:415–26
Toft S, Hjorth J, Burud I. 2000. *Astron. Astrophys.* 356:115–19

Treffers R, Cohen M. 1974. *Ap. J.* 188:545–52
Trumpler RJ. 1930. *Publ. Astron. Soc. Pac.* 42:214–27
Udalski A. 2002. astro-ph/ 0210367v1
van der Hucht KA, Morris PW, Williams PM, Setia Gunawan DYA, Beintema DA, et al. 1996. *Astron. Astrophys.* 315:L193–96
Voshchinnikov NV. 2002. In *Optics of Cosmic Dust*, ed. G Videen, M Kocifaj, pp. 1–36. Dordrecht: Kluwer
Wada S, Kaito C, Kimura S, Ono H, Tokunaga AT. 1999. *Astron. Astrophys.* 345: 259–64
Waelkens C, Malfait K, Waters LBFM. 2000. In *IAU Symp. 197, Astrochemistry*, ed. YC Minh, EF van Dishoeck, pp. 435–46. San Francisco: Astron. Soc. Pac.
Webster A. 1993. *MNRAS* 264:L1–2
Weingartner JC, Draine BT. 2001a. *Ap. J.* 548:296–309 (WD01)
Weingartner JC, Draine BT. 2001b. *Ap. J.* 553:581–94
Weingartner JC, Draine BT. 2003. *Ap. J.* 589:289–318
Welty DE, Fowler JR. 1992. *Ap. J.* 393:193–205
Whittet DCB. 1988. In *Dust in the Universe* ed. ME Bailey, DA Williams, pp. 25–53. Cambridge: Cambridge Univ. Press
Whittet DCB. 2003. *Dust in the Galactic Environment*. Bristol: *Inst. Phys.* 2nd ed.
Whittet DCB, Bode MF, Longmore AJ, Adamson AJ, McFadzean AD, et al. 1988. *MNRAS* 233:321–36
Whittet DCB, Boogert ACA, Gerakines PA, Schutte W, Tielens AGGM, et al. 1997. *Ap. J.* 490:729–34
Whittet DCB, Duley WW, Martin PG. 1990. *MNRAS* 244:427–31
Whittet DCB, Martin PG, Fitzpatrick EL, Massa D. 1993. *Ap. J.* 408:573–78
Wilking BA, Lebofsky MJ, Rieke GH. 1982. *Astron. J.* 87:695–97
Witt AN. 2000a. *J. Geophys. Res.* 105:10299–302
Witt AN. 2000b. In *IAU Symp. 197, Astrochemistry*, ed. YC Minh, EF van Dishoeck, pp. 317–30. San Francisco: Astron. Soc. Pac.
Witt AN, Boroson TA. 1990. *Ap. J.* 355:182–89
Witt AN, Friedmann BC, Sasseen TP. 1997. *Ap. J.* 481:809–20
Witt AN, Gordon KD, Furton DG. 1998. *Ap. J.* 501:L111–15
Witt AN, Oliveri MV, Schild RE. 1990. *Ap. J.* 99:888–97
Witt AN, Petersohn JK, Bohlin RC, O'Connell RW, Roberts MS, et al. 1992. *Ap. J. Lett.* 395:L5–L8
Witt AN, Petersohn JK, Holberg JB, Murthy J, Dring A, Henry RC. 1993. *Ap. J.* 410:714–18
Witt AN, Schild RE. 1985. *Ap. J.* 294:225–30
Witt AN, Schild RE. 1988. *Ap. J.* 325:837–45
Witt AN, Smith RK, Dwek E. 2001. *Ap. J.* 550:L201–5
Witt AN, Walker GAH, Bohlin RC, Stecher TP. 1982. *Ap. J.* 261:492–509
Wolff MJ, Clayton GC, Kim SH, Martin PG, Anderson CM. 1997. *Ap. J.* 478:395–402
Woo JW, Clark GW, Day CSR, Nagase F, Takeshima T. 1994. *Ap. J. Lett.* 436:L5–8